



Lithium isotope evidence shows Devonian afforestation may have significantly altered the global silicate weathering regime

Xianyi Liu^{a,b,*}, Alexander J. Krause^{a,c,d}, David J. Wilson^a, Wesley T. Fraser^e, Michael M. Joachimski^f, Uwe Brand^g, Alycia L. Stigall^h, Wenkun Qieⁱ, Bo Chen^j, Xiangrong Yang^j, Philip A.E. Pogge von Strandmann^{a,k}

^a LOGIC, Department of Earth Sciences, University College London, London WC1E 6BT, UK

^b Department of Earth Science, Utrecht University, Utrecht, 3584 CS, The Netherlands

^c Department of Earth Science, Leeds University, UK

^d School of Earth and Environmental Sciences, Cardiff University, Cardiff CF10 3AT, UK

^e Geography, Department of Social Sciences, Oxford Brookes University, Oxford OX3 0BP, UK

^f GeoZentrum Nordbayern, Friedrich-Alexander-Universität Erlangen-Nürnberg, 91054 Erlangen, Germany

^g Department of Earth Sciences, Brock University, St. Catharines, Ontario L2S 3A1, Canada

^h Department of Earth, Environmental, and Planetary Sciences, University of Tennessee, Knoxville, TN 37922, United States

ⁱ State Key Laboratory of Palaeobiology and Stratigraphy and Center for Excellence in Life and Palaeoenvironment, Nanjing Institute of Geology and Palaeontology, Chinese Academy of Sciences, Nanjing 210008, China

^j Key Laboratory of Tectonics and Petroleum Resources of Ministry of Education, China University of Geosciences, Wuhan 430074, China

^k MIGHTY, Institute of Geosciences, Johannes Gutenberg University, 55122 Mainz, Germany

ARTICLE INFO

Associate editor: Matthew S Fantle

Keywords:

Li isotopes
Devonian
Biosphere
Weathering
Carbonate diagenesis

ABSTRACT

The Devonian Period (~359–419 Ma) documents significant environmental changes and marine species turnover, but whether these changes were linked to terrestrial weathering remains unknown. Here, we use lithium isotopes in brachiopods and bulk marine carbonates ($\delta^7\text{Li}_{\text{carb}}$) from the Devonian Period to investigate changes in silicate weathering, which represents the primary long-term atmospheric CO_2 sink. A rise of ~10‰ in $\delta^7\text{Li}_{\text{carb}}$ values (from ~8‰ to ~18‰) is observed across the Mid-Devonian (~378–385 Ma), suggesting a major change in the seawater Li cycle. We attribute the rise in $\delta^7\text{Li}_{\text{carb}}$ values to an increase in the dissolved riverine Li flux and $\delta^7\text{Li}_{\text{river}}$ values, which likely arose from increases in both weathering intensity and regolith thickness, related to the expansion of deep-rooted plants. However, the presence of such terrestrial ecosystems would also have restricted the continuous weathering of silicate rocks. In order to maintain high $\delta^7\text{Li}_{\text{seawater}}$ values in the Late Devonian, we propose that repeated cycles of destruction and regeneration of terrestrial forest ecosystems could have occurred, which would have prevented a supply-limited weathering regime from being permanently established. Such a process would potentially have caused oscillations in marine nutrient availability and redox conditions, thereby contributing to prolonged marine biodiversity loss during the Late Devonian.

1. Introduction

The Earth during the Devonian Period (~359–419 Ma) experienced significant shifts in both the climate and environment, which left long-lasting impacts on global biogeochemical cycles, which can still be felt during the present day (Becker et al., 2016). For example, a wide range of studies have suggested that there could have been decreases in atmospheric CO_2 (from 2000 ppm to less than 1000 ppm) and increases in O_2 concentrations, which would have been beneficial in creating more

habitable niches for multicellular biota (e.g., Copper and Scotese, 2003; Foster et al., 2017; Lenton et al., 2016). Indeed, during this period, reef construction reached an unprecedented peak, fish diversity increased substantially, and terrestrial plants evolved into forms with more megaphyll leaves, seeds, and roots (Becker et al., 2016; Chen et al., 2021). However, despite these ‘favourable’ conditions, the Late Devonian contains a series of short biological events and biodiversity crises, including the Frasnian-Famennian boundary (F-F, or Kellwasser crisis, ~372 Ma) and the Devonian-Carboniferous boundary (DCB, or

* Corresponding author at: Department of Earth Science, Utrecht University, Utrecht, 3584 CS, The Netherlands.

E-mail address: x.liu6@uu.nl (X. Liu).

<https://doi.org/10.1016/j.gca.2025.02.036>

Received 21 April 2024; Accepted 28 February 2025

Available online 1 March 2025

0016-7037/© 2025 The Author(s). Published by Elsevier Ltd. This is an open access article under the CC BY license (<http://creativecommons.org/licenses/by/4.0/>).

Hangenberg crisis, ~360 Ma), collectively leading to one of the ‘big five’ mass extinctions in geological history which wiped out approximately half of the marine genera (Becker et al., 2020). The direct causes of these events have been extensively debated, with hypothesised mechanisms including: temperature change (Joachimski and Buggisch, 2002); competition from generalists (species) (Stigall, 2012); and toxic aerosols emitted by bolide impacts and volcanism (Barash, 2016). Another potential direct driver for the biodiversity crises may have been ocean anoxia, based on recent evidence from sophisticated biogeochemical models and uranium isotopes (Elrick et al., 2022; Smart et al., 2023). Changes in ocean redox conditions at this time were likely linked to tectonic activity (both volcanism and mountain building) and/or plant evolution events, both of which could significantly change continental weathering processes (e.g., Algeo and Scheckler, 1998; Chen et al., 2021; McGhee and Racki, 2012; Willis and McElwain, 2014).

However, there is only limited direct evidence showing (1) how and why weathering processes might have changed during this time, (2) the influence weathering could have had on the operation of the Earth system, and (3) its consequent impacts on the Devonian mass extinctions (e.g., Percival et al., 2019). Efforts to solve these problems have included investigations of radiogenic strontium (Sr) isotopes in paleo-seawater archives (e.g., van Geldern et al., 2006), but such records are not exclusive in recording silicate weathering, being obscured by hydrothermal fluxes (Pogge von Strandmann et al., 2013) and carbonate weathering, which does not directly influence climate on timescales greater than tens of thousands of years. Therefore, other proxies are needed to trace silicate weathering throughout the Devonian Period.

Lithium isotopes ($\delta^7\text{Li}$) are a robust tool for studying silicate weathering processes, since Li is mainly hosted in silicate minerals (Penniston-Dorland et al., 2017). Lithium has two isotopes: ^7Li and ^6Li . During the dissolution of primary rocks, Li isotopes are not significantly fractionated, i.e., the dissolved fluid has an identical $\delta^7\text{Li}$ value to primary silicate rocks (Pistiner and Henderson, 2003). In contrast, the formation of secondary minerals (e.g., clays, oxides) strongly fractionates Li isotopes, with a preference for ^6Li incorporation in the solid (Hindshaw et al., 2019; Vigier et al., 2008). Surface water Li isotopes are not significantly fractionated by vegetation uptake or organic complexation (Pogge von Strandmann et al., 2022). Recent studies have linked the fractionation of Li isotopes to the water–rock interaction time (Dellinger et al., 2015; Zhang et al., 2022a). In the modern ocean, Li has a residence time of ~ 1 Myr, and is mainly supplied by continental weathering and hydrothermal on-axis circulation fluids (e.g., Pogge von Strandmann et al., 2013). Lithium is removed from seawater by clay mineral formation, in both shallow marine sediments and deep marine off-axis oceanic crust (e.g., Li and West, 2014; Zhang et al., 2022b). Therefore, if the sinks and the hydrothermal inputs can be constrained, paleo-seawater Li isotope compositions can be interpreted in terms of paleo-continental weathering. Indeed, Li isotopes in bulk carbonates or foraminifera have been successfully applied to trace changes in terrestrial weathering processes in previous studies (e.g., Hathorne and James, 2006; Kalderon-Asael et al., 2021; Misra and Froelich, 2012; Pogge von Strandmann et al., 2013). Hence, we suggest that Li isotopes could be a reliable tracer for examining silicate weathering processes during the Devonian.

Here, we report $\delta^7\text{Li}$ data from brachiopods and bulk carbonates across the Devonian Period to track changes in silicate weathering. These samples were collected from a range of global sites with different depositional settings (Tables S1 and S2). To date, only a handful of studies have been conducted on brachiopod carbonates for Li isotopes, and they have suggested that brachiopods can faithfully record marine Li isotopes with a constant isotopic offset between carbonates and seawater (e.g., Washington et al., 2020). We further assess the fidelity of Palaeozoic brachiopods for recording seawater Li isotope compositions. We then determine whether silicate weathering changed during this period or not, and examine the possible mechanisms driving the observed $\delta^7\text{Li}$ variations during the Devonian. Finally, we consider the

implications for the role of weathering in Late Devonian mass extinctions and the operation of the Earth system.

2. Materials and Methods

2.1. Sample collection

We obtained 73 brachiopod samples covering most of the Devonian Period from the collections of Brand (1989), van Geldern et al. (2006), and Rode and Lieberman (2004) (Table S1). The samples from Brand (1989) and van Geldern et al. (2006) have previously been tested using cathodoluminescence and used to generate oxygen (O) and carbon (C) isotope data, while no geochemical data has previously been reported from the samples of Rode and Lieberman (2004). The sampling locations are shown in Fig. 1 and the species and ages are listed in Table S1. The ages of samples were estimated from conodont zones, with samples from the Emsian, and from the Givetian to the Famennian (Fig. 2, Table S1). An additional 17 mid-deep water bulk carbonate (limestone) samples that were deposited in a rift basin were collected in South China to provide a comparison with the brachiopod samples (Fig. 1, Table S2). The ages of the bulk carbonate samples range from 419 Ma to 363 Ma, covering the majority of the Devonian (except for a gap in the Emsian) (Fig. 2, Table S2). The aim of this sampling approach is to compare data from different regions and different carbonate types, in order to filter for the effect of diagenetic alteration.

2.2. Analysis

Samples from two sources have existing O and C isotope data (Brand, 1989; van Geldern et al., 2006), while the O and C isotope data for the samples from Rode and Lieberman (2004) were newly obtained at the Bloomsbury Environmental Isotope Facility (BEIF) using a Finnigan Delta Plus XP mass spectrometer (Thermo Fisher Scientific, Waltham, MA, USA). The precision of all internal (BDH, IAEA, and IFC) and external standards (NBS19) was $\pm 0.02\text{‰}$ for $\delta^{13}\text{C}$ and $\pm 0.04\text{‰}$ for $\delta^{18}\text{O}$.

Samples were rinsed with 18.2 M Ω cm (MQ) water to remove any dust on the surface. They were then either drilled by micro-drill or peeled off using a VOMM $\text{\textcircled{C}}$ metal spatula. The peeled-off samples were ground to a fine powder using an agate mortar and pestle. All samples were transferred to 2 mL centrifuge tubes and rinsed twice with MQ water, before being leached with 0.1 M HCl for one hour at room temperature (Pogge von Strandmann et al., 2019b). The amount of acid added was calculated to ensure digestion of less than 90 % of the carbonate. The tubes with the carbonate leachates were then centrifuged for 3 min (11,000 RPM), and the supernatants were carefully pipetted off and dried down in PFA beakers on a PFA-coated hotplate at 130 $^{\circ}\text{C}$ in a Class 100 metal-free clean room.

For measurements of elemental concentrations, 100 μL of supernatant was diluted to approximately 50 $\mu\text{g/g}$ calcium (Ca) in 2 % HNO_3 and analysed on a Varian 720 Inductively Coupled Plasma Optical Emission Spectrometer (ICP-OES) and an Agilent 7900 quadrupole Inductively Coupled Plasma Mass Spectrometer (ICP-MS) in the LOGIC laboratories at UCL. A series of multi-elemental synthetic solutions covering a wide range of concentrations was prepared from Agilent $\text{\textcircled{C}}$ single standard solutions and used to calibrate the measurements. The USGS SGR-1 standard was used to assess the quality of the calibration. Analytical precision was better than $\pm 2\%$ for OES measurements and $\pm 5\%$ for ICP-MS measurements for the analysed elements (Table S1 and S2).

After the carbonate leachates were dried, they were loaded onto columns filled with AG50W X-12 resin and purified following a two-stage cation exchange column procedure using 0.2 M HCl as the eluant (Pogge von Strandmann et al., 2019a). Because Li isotopes are fractionated during cation exchange, a Li recovery of more than 99.8 % should be ensured for all samples. Atlantic seawater and blank samples

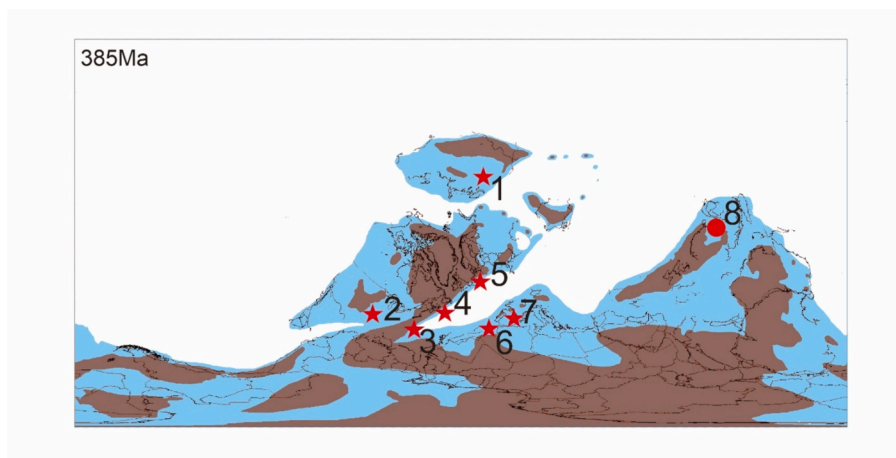


Fig. 1. Location map for samples used in this study. Red stars and red circle are the locations of brachiopod samples and bulk samples, respectively. 1- Siberian; 2- Mid-West United States (Ohio, Missouri, Nevada, and Montana State); 3- New York State (Appalachian Mountains); 4- Canada (Appalachian Mountains); 5- Germany; 6- Morocco; 7- Spain; 8- South China. The base map is modified from PALEOMAP (<http://www.scotese.com>) at 385 Ma. The blue areas in the map are shallow marine, and brown areas are continents.

were processed together with the samples to provide a further control for the accuracy and precision of the data. Purified samples were analysed for Li isotopes using a Nu Plasma 3 multi-collector inductively coupled plasma mass spectrometer (MC-ICP-MS) in the UCL LOGIC laboratories, by sample-standard bracketing with the IRMM-016 standard. The measured $\delta^7\text{Li}$ values were converted to values based on L-SVEC, where $\Delta^7\text{Li}_{\text{IRMM to L-SVEC}} = -0.003 \pm 0.054\text{‰}$. Analytical details are given in Pogge von Strandmann et al. (2019a). The long-term reproducibility of seawater $\delta^7\text{Li}$ values in this study is $30.95 \pm 0.49\text{‰}$ (2sd, $n = 6$), in good agreement with published values (Penniston-Dorland et al., 2017; Pogge von Strandmann et al., 2019a).

3. Results

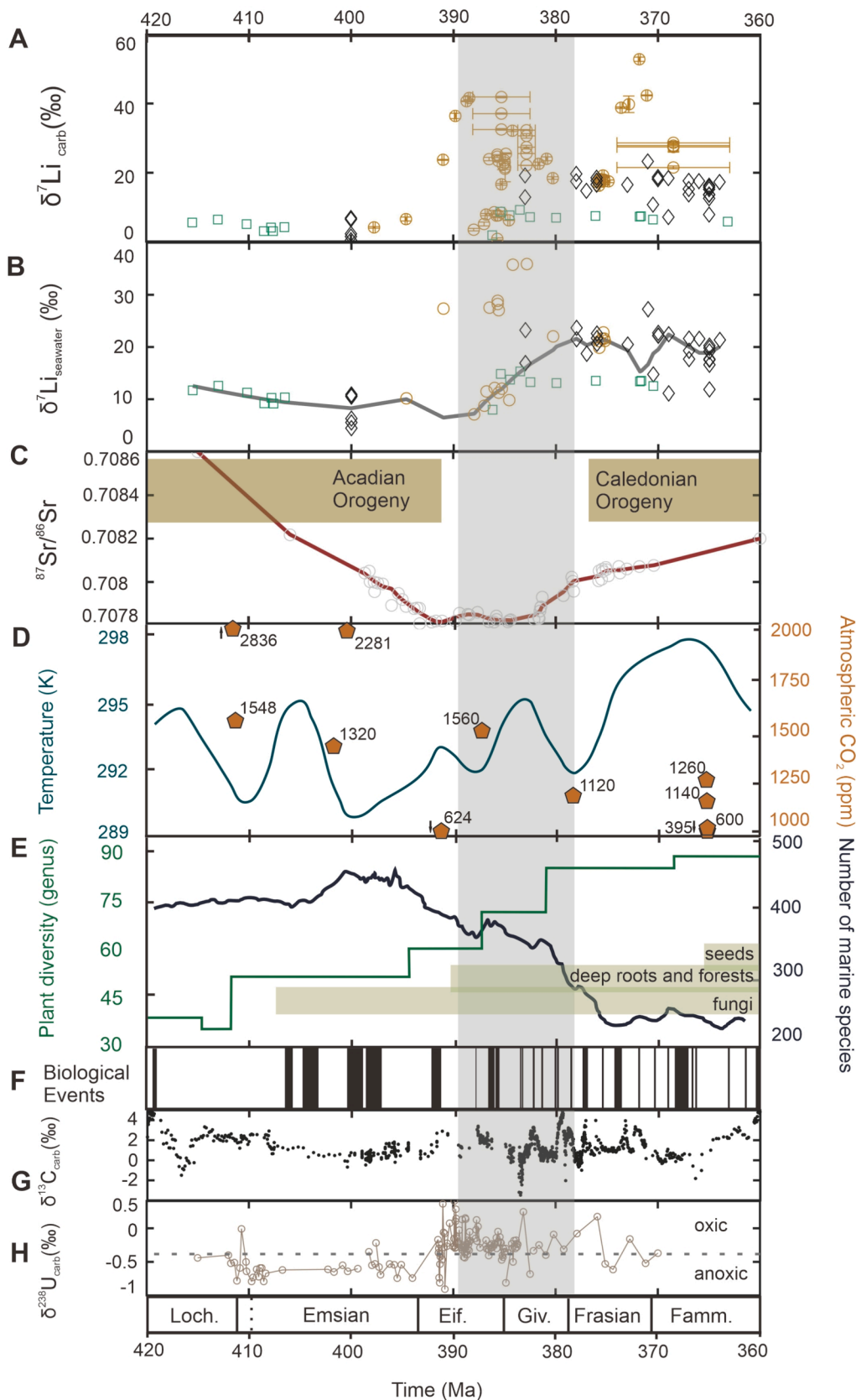
Our new dataset for all measured samples shows an increase in Li isotope compositions across the Devonian, in both brachiopods and bulk carbonates (Fig. 2A, Tables S1 and S2). After applying diagenetic screening methods (see Discussion) and converting $\delta^7\text{Li}_{\text{carb}}$ to $\delta^7\text{Li}_{\text{seawater}}$ values (see below), this increasing pattern remains (Fig. 2B). Generally, the $\delta^7\text{Li}$ values of brachiopods (and hence inferred seawater) increased by $\sim 10\text{‰}$ from the Early to Late Devonian (Fig. 2B). Before the Mid-Devonian (385 Ma), the $\delta^7\text{Li}_{\text{carb}}$ values ranged from 6 to 10‰, with an average of 8‰. The $\delta^7\text{Li}_{\text{carb}}$ values then increased to $\sim 18\text{‰}$ after the Mid-Devonian, with a more variable range (~ 10 to 20‰). The increase occurred in a short interval of ~ 10 Myr, approximately from 390 to 380 Ma (grey bar in Fig. 2B). A Student's *t*-test suggests resolvable differences between the $\delta^7\text{Li}$ values before and after 385 Ma (p -value = 0.00018, degrees of freedom = 67). Assuming that the brachiopod carbonate archive has a constant negative offset of 3.6‰, and bulk carbonates of 6.1‰, from seawater $\delta^7\text{Li}$ values at the time of deposition (Dellinger et al., 2018; Pogge von Strandmann et al., 2019b; Washington et al., 2020), $\delta^7\text{Li}_{\text{seawater}}$ can be reconstructed by adding those offset values onto the $\delta^7\text{Li}_{\text{carb}}$ data (Kalderon-Asael et al., 2021) (Fig. 2B). The $\delta^7\text{Li}_{\text{seawater}}$ curve is fitted with a robust LOESS method in MATLAB 2020a (Fig. 2B, Fig. S8). Our new data is in general agreement with the low-resolution Phanerozoic data from Kalderon-Asael et al. (2021) who also reported a rising trend in $\delta^7\text{Li}$ values during the Palaeozoic.

4. Discussion

4.1. Are brachiopods a good archive for past seawater Li isotope compositions?

Given that modern brachiopods display limited intra-shell and inter-species differences and have a relatively small and constant Li isotope fractionation (-3.6 to -4.2‰) from the culturing fluid (Dellinger et al., 2018), brachiopod fossil carbonates are regarded as a potentially useful archive to record paleo-seawater chemistry (Washington et al., 2020), but must be carefully screened for potential diagenetic alteration. As there is no single method to screen for the fidelity of the geochemical composition in fossil brachiopod samples, here we used two methods to assess the extent of alteration: (1) optical microscopy, and (2) geochemical filtering (e.g., Ullmann and Korte, 2015).

Before assessing sample diagenesis, we used elemental ratios as a geochemical tool to assess the validity of the acid leaching. This test is necessary because silicate minerals (including primary silicate minerals and secondary silicate minerals) are enriched in lithium (Li) compared to carbonates, so even a small amount of silicate contamination (i.e., mud from the host rocks) could overprint the primary carbonate $\delta^7\text{Li}$ signal in the brachiopods. Silicates generally have low $\delta^7\text{Li}$ values (close to 0‰), so if the carbonate leachates are contaminated, the resulting $\delta^7\text{Li}$ values should be driven lower. Aluminium/calcium (Al/Ca) ratios are widely used to assess potential contamination from the leaching of silicate minerals, because Al is a major element in silicate minerals, while its concentrations are negligible in pure carbonate minerals (Kalderon-Asael et al., 2021; Pogge von Strandmann et al., 2013; Washington et al., 2020). We observed no general trend between Al/Ca ratios and $\delta^7\text{Li}$ values in all samples, potentially suggesting limited effects from silicate contamination (Fig. 3A). However, when dividing the samples according to their host-rock lithology (shale, carbonate, shaley carbonate), we find that for the shale-hosted samples, there is a subtle decreasing trend in Li isotopes versus Al/Ca ratios when Al/Ca > 0.8 mmol/mol. This threshold is the same as the cut-off Al/Ca ratio of 0.8 mmol/mol previously reported (Pogge von Strandmann et al., 2013), which has been extensively applied in many previous studies (Bastian et al., 2018; Kalderon-Asael et al., 2021; Pogge von Strandmann et al., 2013; Washington et al., 2020). Meanwhile, these samples also showed elevated Li/Ca ratios, further suggesting contamination from silicate minerals (Fig. 3B). Overall, 14 samples were excluded due to potential silicate contamination on the basis of their Al/Ca ratios (Fig. 3A, B). We further plotted the expected end-members of pure brachiopod



(caption on next page)

Fig. 2. Lithium isotopes and other data from the Devonian Period. A: All Li isotope data from carbonates obtained in this study. Brown circles are data from brachiopods (this study), green squares are data from bulk carbonates (this study), and black diamonds are data from [Kalderon-Asael et al. \(2021\)](#) (including bulk carbonates and brachiopods). B: Li isotope data that passed the diagenesis screening procedure, converted to seawater values (see text for fractionation factors). The grey curve is a robust LOESS curve, smoothed using a smoothing factor of 0.2 (see Fig. S8 for alternative curves). C: Radiogenic Sr isotope data from the seawater archives of [van Geldern et al. \(2006\)](#) and [McArthur et al. \(2020\)](#). The two brown bars represent two major Devonian orogeny events ([Chen et al., 2021](#)) that coincided with elevated Sr isotope compositions. D: Temperature reconstruction (dark green line), modified from previous studies ([Scotese et al., 2021](#)). Atmospheric CO₂ reconstructions (brown pentagons) from [Foster et al. \(2017\)](#), with the adjacent numbers giving the estimated values. E: Terrestrial plant diversity (green line; [Cascales-Miñana, 2016](#)), and the numbers of marine animal species (black line; [Fan et al., 2020](#)). The green bars show the major innovations in terrestrial plants ([Willis and McElwain, 2014](#)). F: Major biological events in the Devonian ([Becker et al., 2020](#)), the frequency of which increased in the Late Devonian. G: Carbon isotope data from carbonates ([Cramer and Jarvis, 2020](#)), which show a higher frequency of oscillations towards the end of the Devonian. H: Uranium isotope data from carbonates ([Elrick et al., 2022](#)), which indicate anoxic seawater in the Early Devonian, and predominately oxic but highly variable seawater oxygenation in the Late Devonian. The grey vertical bar across all panels indicates the Mid-Devonian shift in Li isotopes.

carbonates and sediments to assess contamination (Fig. 3A, B), although the chemistry of the end-members is highly uncertain. For the case of extremely high initial carbonate Li isotope compositions of 60 ‰, the samples screened with 0.8 mmol/mol cut-offs sit on mixing lines towards the sediments, suggesting the validity of this cut-off.

To assess diagenesis by optical microscopy, we followed a protocol employed by [McArthur et al. \(2012\)](#), using a small VOOOM® metal spatula to peel off the brachiopod shells onto weighing papers for scrutinization. We would expect to observe certain features as signs of ‘good preservation’, including (1) translucent and light colour; (2) original shell-like shape, flakiness, and lineation (i.e., primary structures remain); and (3) vitreous lustre (Fig. S1 A-D). If the primary low-magnesium calcite (LMC) brachiopods were dissolved and recrystallized, the new abiotic calcite would generally lose the primary structures of the original biogenic calcite. Compared to SEM inspection, optical microscopy can avoid observational biases which may arise from sample heterogeneity when viewing only a small portion of the sample ([Ullmann and Korte, 2015](#)). However, because some samples were not large enough to be peeled by spatula, we could only apply this method in limited cases, with only 28 samples being assessed in this way (Table S1, ‘Microscope’ column), and 7 samples did not meet these criteria. However, this method is not fully quantitative, and therefore was combined with geochemical screening.

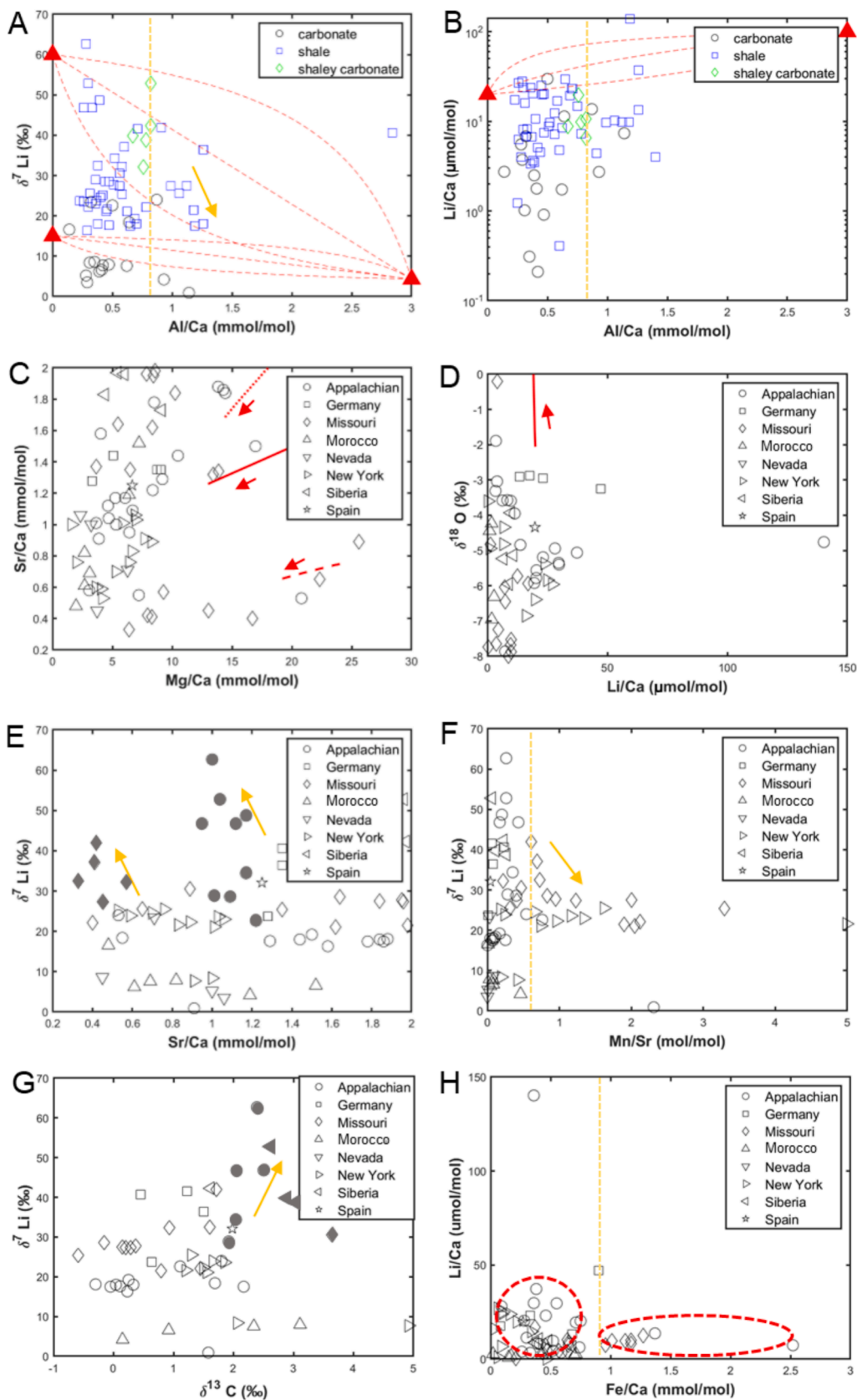
Due to a limited understanding of diagenetic processes, shell growth rates, and ancient seawater compositions, debates are ongoing in terms of the choice of geochemical filters and appropriate cut-off values for diagenetic alteration in fossil samples ([Ullmann and Korte, 2015](#)). Also, the alteration of elements with a short reactive length scale in pure carbonate settings (e.g., Ca) may not be a useful tracer for elements with longer reactive length scales (e.g., Sr), implying that it is important to select multiple appropriate diagenesis proxies, favouring elements with similar reactive length scales ([Fantle et al., 2020](#)). Previous research on the diagenesis of fossil samples in sediments suggests that Li isotopes might be significantly altered during recrystallisation ([Andrews et al., 2020](#); [Fantle et al., 2020](#); [Ullmann et al., 2013](#)). Metal elements (Mn and Fe) have been proposed as diagenetic (recrystallisation) proxies ([Brand, 1989](#); [Fantle et al., 2020](#); [van Geldern et al., 2006](#); [Washington et al., 2020](#)), because Mn and Fe can be incorporated into recrystallised carbonate from reduced fluids. Given that the samples from [Rode and Lieberman \(2004\)](#) contain large amounts of pyrite, which might imply reduced fluid conditions, Mn and Fe are included in the analysis. Brachiopods typically have a low Mn and Fe content; therefore, observations of high concentrations would likely indicate interactions with reduced fluids bearing high Mn and Fe concentrations ([Ullmann and Korte, 2015](#)). Strontium can also be lost during the carbonate dissolution-recrystallisation process, while high Mg contents may indicate potential dolomitization ([Ullmann and Korte, 2015](#)).

We selected a series of widely used diagenesis proxies, based on the elements that should indicate recrystallisation processes, including Mg/Ca, Sr/Ca, Mn/Sr, Fe/Ca, and oxygen isotopes ([Fantle et al., 2020](#); [Ullmann and Korte, 2015](#); [Washington et al., 2020](#)), to compare to the Li concentrations or Li isotopes (Fig. 3). The trends among these proxies can serve as evidence for diagenesis. If no trends were observed, we set

the expectations for the initial chemical composition based on modern brachiopod studies ([Dellinger et al., 2018](#); [Ullmann et al., 2017](#)) (Table S3) and ran a diagenesis model, comparing the simulation results with the samples (Supplementary Materials) ([Fantle and Lloyd, 2025](#)). The diagenesis model employs reactive transport modelling to determine how the elemental and isotopic compositions would have changed during the process of carbonate recrystallisation, with given initial conditions and partition coefficients (the parameters and assumptions can be found in the Supplementary Materials). However, in a multi-reactive phase system, such as brachiopods hosted in shale, both silicate and carbonate minerals are reacting in the sediments, with implications for the behaviour of Li. Because Li has low concentrations in fluids and carbonates, but has a high partition coefficient into silicate minerals, it might have longer reactive length scales than the above (diagenetic proxy) elements, so there is a chance that the Li concentration and/or isotopic composition of a sample could be altered without signs of alteration in the proxies with shorter reactive length scales ([Penniston-Dorland et al., 2017](#); [Fantle and Lloyd, 2025](#)). Therefore, we do not use these major element proxies to make any firm conclusions regarding whether samples have been diagenetically altered or not, only that Li is more likely to have been diagenetically altered in certain samples.

A cross-plot between Mg/Ca and Sr/Ca ratios (Fig. 3C), as an indicator for recrystallisation, shows positive trends for some samples (potentially suggesting diagenesis for some samples), although both Mg/Ca and Sr/Ca ratios are within the range of modern brachiopods (Table S3). We select three initial carbonate conditions (see Supplementary Materials for details) and run the diagenesis model to simulate how the carbonate chemistry would be altered ([Fantle and Lloyd, 2025](#)). We do not intend to use this model to represent all possibilities, but rather to illustrate some possible scenarios. The diagenetic trajectories suggest that as recrystallisation proceeds, samples would gradually lose Mg and Sr relative to Ca, but the range of chemical variation observed between the samples cannot be fully explained by the diffusion-dominated recrystallisation process by starting with certain initial values. However, subtle positive trends in some sample sets (Fig. 3C, red arrows) and model runs (Fig. 3C, red lines) may suggest that at least the Canadian Appalachian and Missouri samples with lower Mg/Ca and Sr/Ca ratios might have undergone recrystallisation. Furthermore, the cross-plot between Sr/Ca ratios and Li isotopes (Fig. 3E) shows that the loss of Sr coincides with elevated Li isotope compositions in the Appalachian (cut-off = ~ 1.2 mmol/mol) and Missouri (cut-off = 0.6 mmol/mol) samples, suggesting that the Li isotopes in these samples might be diagenetically altered ([Ullmann et al., 2013](#)).

Diagenesis of some samples is further confirmed in other proxies. Lithium isotopes begin to show a decreasing trend beyond our cut-off of Mn/Sr = 0.6 mmol/mol (Fig. 3F), and there is a rough negative trend between Li/Ca and O isotopes for the Canadian Appalachian samples (Fig. 3D, circles). There are also subtle positive trends in the Li/Ca versus Fe/Ca cross-plot at high Fe/Ca values (Fig. 3H), which yields a threshold of 0.9 mmol/mol (the samples are mainly clustered in two groups and Fe/Ca = 0.9 mmol/mol is the cut-off to separate them), which is similar to the upper limit of the Fe/Ca range in modern brachiopods (Fig. 3H);



(caption on next page)

Fig. 3. Diagenesis assessment using geochemical proxies. A: Li isotopes versus Al/Ca ratios to assess potential silicate contamination. The yellow arrow indicates a potential silicate contamination trend. The red dashed lines are mixing lines with $r = 0.2, 1, 5$, starting from two sets of end-members (represented by red triangles). The value of r determines the curvature of the mixing line; for its definitions and the mixing line equations see Langmuir et al. (1978) and the Supplementary Materials. The end-members have Li isotope compositions of 60 ‰ or 15 ‰ with Al/Ca = 0, representing pure brachiopod carbonates, and a Li isotope composition of 4 ‰ with Al/Ca = 3 mmol/mol, representing shale residues (Pogge von Strandmann et al., 2013). The yellow dashed line is the cut-off adopted in the setting, and samples beyond this line were excluded. B: Li/Ca versus Al/Ca ratios. The red dashed lines are the mixing lines with $r = 0.2, 1, 5$, between carbonate and shale end-members (represented by red triangles). The yellow dashed line is the cut-off adopted in the setting, and samples beyond this line were excluded. C: Sr/Ca versus Mg/Ca ratios to trace potential recrystallisation. The three red lines represent three exemplar results from a diagenesis model (see main text), and the red arrows indicate the diagenetic trajectories. D: O isotopes versus Li/Ca ratios. The red line indicates the results from the diagenesis model, and the red arrow indicates the diagenetic trajectory. E: Li isotopes versus Sr/Ca ratios. The yellow arrows indicate potential diagenetic trends. The filled markers indicate samples that were excluded based on this cross-plot. F: Li isotopes versus Mn/Sr ratios. The yellow arrow indicates potential diagenetic trends. The yellow dashed line is the cut-off adopted in the setting, and samples beyond this line were excluded. G: Li isotopes versus C isotopes. The yellow arrow indicates potential diagenetic trends. The filled markers indicate samples that were excluded based on this cross-plot. H: Li isotopes versus Fe/Ca ratios. The yellow dashed line is the cut-off adopted in the setting, and samples beyond this line were excluded. The label ‘Appalachian’ in the legend means Canadian Appalachian.

Table S3). All samples have C isotope compositions within the range of modern brachiopods, but there is a slight increasing trend between Li and C isotopes (Fig. 3G), potentially implying that they might be diagenetically altered (Ullmann et al., 2013). Overall, the multi-proxy diagenetic filtering helps rule out a further 30 samples (Table S1) on top of the clay contamination screening and microscopy screening (44 samples ruled out in total).

Eighteen of the total unscreened brachiopod samples show high $\delta^7\text{Li}$ values (values > 31 ‰, the modern seawater value) (Fig. 2A). Similar, exceptionally high Li isotope compositions, have also been reported in previous studies and likely result from diagenesis (Andrews et al., 2020; Kalderon-Asael et al., 2021). These high $\delta^7\text{Li}$ values are unlikely to reflect vital effects, because the $\Delta^7\text{Li}_{\text{calcite-seawater}}$ values in modern brachiopods are small, with little variation among species, and with no clear relationship between species and $\delta^7\text{Li}$ values (Dellinger et al., 2018). Furthermore, these high values are also unlikely to reflect original seawater signals for three reasons:

- (1) The samples with high $\delta^7\text{Li}$ values generally have lower Li/Ca ratios (Table S1) than the range for unaltered brachiopods (Li/Ca = 15–50 $\mu\text{mol/mol}$) (Dellinger et al., 2020) (Table S3). The lower Li/Ca ratios suggest that the brachiopods may have experienced diagenetic alteration leading to Li loss and/or exchange that may potentially change Li isotope compositions (Dellinger et al., 2020).
- (2) If brachiopod $\delta^7\text{Li}$ values as high as 58 ‰ (Fig. 2A) were to reflect an original signal, then the global seawater Li budget would have needed some combination of the following extreme scenarios: a significantly muted hydrothermal Li input, as this is a source of isotopically light Li (Hathorne and James, 2006); an isotopically heavy global riverine flux (considerably more extreme than seen in modern rivers); and a greater degree of isotopic fractionation ($\Delta^7\text{Li}_{\text{seawater-sink}}$) during removal into the oceanic Li sinks (altered oceanic crust (AOC) and marine authigenic aluminosilicate clays (MAAC)) (Li and West, 2014; Zhang et al., 2021). However, there is little evidence that any of these pathways were in place during the Devonian period (Kalderon-Asael et al., 2021; Mills et al., 2017; Williams et al., 2021).
- (3) The samples with high $\delta^7\text{Li}$ values are particularly common in a few locations (e.g., samples labelled with YA from Siberia, or STR from Germany; Table S1), suggesting the possibility of local post-depositional diagenetic overprinting.

Most of the samples (16 out of 18) with high $\delta^7\text{Li}$ values were determined to be diagenetically altered by our geochemical diagenesis filtering process (see above) and were ruled out for further analysis (Table S3, Fig. 2). The remaining two samples are not excluded from further analysis.

We hypothesise that the high $\delta^7\text{Li}$ values in those altered samples could be due to alteration of calcite by pore waters during early diagenesis in a clay-carbonate dual system (e.g., Andrews et al., 2020;

Dellinger et al., 2020; Pogge von Strandmann et al., 2019b). Such a system has been extensively investigated by dual-system diagenesis modelling (e.g., Andrews et al., 2020; Fantle et al., 2020). The key finding from these studies is that, considering the rate of clay authigenesis (and therefore the rate of Li removal) in pore water outcompetes the effect from diffusion (Chanda et al., 2023), the dissolution/authigenesis of clay should dominate the Li concentrations and isotopic compositions in the pore fluid, thereby taking them out of an equilibrium state with regard to the carbonate. That is to say, in pore water, ^6Li is preferentially incorporated into authigenic clays (or other secondary minerals), leaving ^7Li enriched in the fluid, along an isotopic-distillation evolution pattern (Andrews et al., 2020; Seyedali et al., 2021). As the chemical composition of carbonate is not in equilibrium with the composition of the pore water, which is altered due to clay authigenesis, the carbonate components (i.e., brachiopods) in the shale may establish a new equilibrium with the pore water via diagenesis and partly inherit this pore water chemistry (e.g., Fig. S1E) (Andrews et al., 2020). On the basis of this theory, if we assume that highly altered samples have low Li contents but high $\delta^7\text{Li}$ values, we would expect a negative trend between $\delta^7\text{Li}$ values and Li/Ca ratios, and this feature is observed for some samples in our dataset (Fig. 4A).

We further used the Li and Na concentrations in the brachiopod calcite (i.e., Li/Na in solid) to calculate the Li/Na values of the pore fluid (i.e., Li/Na in fluid) in which the carbonate was precipitated (Füger et al., 2019) (Fig. 4B). This approach is feasible because both Li and Na are monovalent trace elements that are associated with the presence of defects on a crystal surface, so have a similar partitioning mechanism. The empirical relationship is as follows:

$$\text{Log} \left(\frac{[\text{Li}/\text{Ca}]_{\text{solid}}}{[\text{Li}/\text{Ca}]_{\text{fluid}}} \right) = 0.707 \text{Log} \left(\frac{[\text{Na}/\text{Ca}]_{\text{solid}}}{[\text{Na}/\text{Ca}]_{\text{fluid}}} \right) - 0.563 \quad (1)$$

We emphasise that this calculation involves several assumptions: it uses Li and Na partition coefficients into carbonate minerals during precipitation under experimental, instead of diagenetic, conditions, and it requires the Na and Ca concentrations of Devonian seawater, which we have adopted from modelled Late Devonian values (Na/Ca = 32 mol/mol) (Demico et al., 2005). Based on those calculations, our altered brachiopod samples can be explained by isotopic distillation with an isotopic fractionation factor (α) of 0.992 (ranging between 0.985 and 0.997), and/or by varying the starting points for the initial Li/Na ratios in the fluid (Fig. 4B). Such a range of fractionation factors agrees with previous studies (Pogge von Strandmann et al., 2019a). The calculated pore fluid Li/Na value is comparable to (or higher than) that of the present-day seawater value, and the screening methods above have successfully ruled out the majority of the abnormally high $\delta^7\text{Li}$ values that could be caused by this process (black sample points in Fig. 4B).

From the above observations, we conclude that caution should be taken when assessing paleo-records from carbonates hosted in silicate-dominated sediments (Andrews et al., 2020). Due to the long reactive length scale of Li in the dual shale-carbonate system, the recrystallised

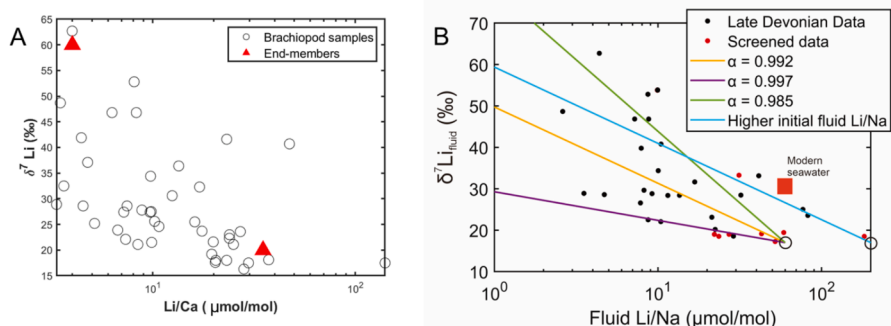


Fig. 4. A: Negative relationship between Li/Ca ratios and Li isotopes in brachiopod samples. The two red triangles represent the ‘initial carbonate’ (bottom right) and the ‘fully altered carbonate’ (top left). B: Reconstructed pore fluid Li/Na ratios and Li isotopes. The dots are data from the Late Devonian (360–385 Ma) brachiopods, where the red dots are the samples which passed the screening for diagenesis, and the black dots are the samples that failed the screening. The red square shows the modern seawater Li/Na ratio and Li isotope composition. The four lines model possible isotopic-distillation evolution pathways, starting from initial fluids with different compositions from today (open black circles). The samples with high $\delta^7\text{Li}$ values can be explained by an isotopic-distillation fractionation with different fractionation factors (0.997, 0.992, 0.985), and/or with varying initial fluid Li/Na compositions (60 $\mu\text{mol/mol}$, 200 $\mu\text{mol/mol}$). The Li/Na ratios of those two initial fluids are determined from the clusters of data points with the highest Li/Na ratios and lowest Li isotope compositions, as we do not know the Li/Na values of seawater in the Devonian. Assuming modern-like seawater Li/Na ratios, the intermediate fit to the data (gold line) is obtained using a fractionation factor of 0.992. The range of fractionation factors could be explained by Li partitioning into different binding sites, the effects of kinetic fractionation, and/or differences in reaction pathways. Note that not all samples are plotted here, since Li/Na ratios were not measured on every sample.

carbonate could have inherited a signal from pore waters which have undergone significant isotopic-distillation processes. Also, in low magnesium carbonate (LMC), Li and other monovalent metals mainly exist in interstitial positions instead of in the mineral lattice (Marriott et al., 2004). Therefore, the porewater and calcite can exchange Li, Na, and other alkali metals even without recrystallising carbonate minerals (Yoshimura et al., 2017).

Generally, our samples have relatively intermediate Al/Ca (0.61 ± 0.39 mmol/mol, $n = 73$), Mn/Sr (0.58 ± 0.52 mmol/mol, $n = 70$), and Fe/Ca (0.52 ± 0.41 mmol/mol, $n = 60$) ratios, but they have high Mn/Ca ratios (0.55 ± 0.85 mmol/mol, $n = 68$). Although optical observation tools can identify some samples which have undergone diagenesis, the geochemical filtering is a more general technique and can more robustly identify samples that display diagenetic signatures (i.e., samples ruled out by optical tools are also ruled out by the geochemical tools). Overall, the combination of our geochemical-based silicate contamination and diagenesis screening ruled out 44 samples (out of 73 samples, 67 of which had Li isotope data), such that 23 samples are considered valid as robust paleo-archives for Li isotopes. By using a strict application of these screening tools, we have good confidence that all the brachiopod samples that have potentially been chemically altered or contaminated have been filtered out. The samples that passed the diagenesis filtering are indicated in Table S1 and are used in the following interpretation.

We emphasise that only 23 out of 73 samples (of which Li isotopes were measured in 67 samples) passed these assessments, and this proportion (~30%) is lower than that reported for Cenozoic brachiopods (~50%) (Washington et al., 2020) and for mixed collections of carbonates (~70%) (Kalderon-Asael et al., 2021). In addition to the impacts of the distillation process described above, the method used here to obtain the carbonate powders (i.e., drilling or peeling off by spatula) could also have contributed to the low pass rate, since the average Al/Ca value from the peeled-off samples was 40% higher than in the drilled samples (0.71 ± 0.25 mmol/mol, $n = 29$ vs. 0.54 ± 0.46 mmol/mol, $n = 42$, respectively). This difference might be because brachiopod fossils embedded in shale bedrock can contain detrital silicate phases (i.e., clays) between the carbonate layers (Fig. S1E), such that the peeling-off method may increase the risk of contamination from non-carbonate minerals. In contrast, the tips of dental drills are small enough to avoid sampling any silicate host rock, so the samples obtained by drilling are less likely to be contaminated.

4.2. Drivers of the increase in Devonian seawater $\delta^7\text{Li}$ values

Our data suggest that Devonian seawater $\delta^7\text{Li}$ values increased by ~10 ‰ around the Givetian Stage (~378–385 Ma) (Fig. 2B). This increase accounts for a large part of the observed rise over the past 3 Ga (Kalderon-Asael et al., 2021), and considerably narrows the timeframe for the major Phanerozoic increase in the seawater Li isotope composition. At first glance, such a monotonic increasing trend contrasts with the variability in the Devonian seawater Sr isotope curve (Fig. 2C), which generally reflects the timing of major orogenic events. As the Sr isotope ratios are considered to be sensitive to variations in hydrothermal activity and/or continental weathering due to orogenic processes (McArthur et al., 2012), the decoupling of Li and Sr isotopes may suggest that the Li isotope record of this study was not predominantly controlled by these two factors. Also, the sustained increase in the Li isotope compositions suggests that the increase is unlikely to have been linked to transient events (e.g., Large Igneous Province eruptions). Instead, the increase may be related to step changes, such as changes in plant evolution, or variations in the composition of the atmosphere. However, a more detailed analysis is needed to understand the actual cause for such a relatively rapid and monotonic change.

To further investigate the drivers of the Devonian Li isotope rise, we used a steady-state isotope mass balance (IMB) to assess the effect of variations in the input and output fluxes of Li on the Devonian Li cycle. We adopted a steady-state approach because the timescale of this study (~60 Myr) is significantly longer than the modern-day residence time of Li (~1 Myr), and because the sample resolution is too low to properly observe non-steady-state changes over shorter timescales (Kalderon-Asael et al., 2021; Li and West, 2014; Misra and Froelich, 2012; Vigier et al., 2015). The IMB model has three inputs (continental weathering, hydrothermal activity, and subduction refluxes) and one combined output (Kalderon-Asael et al., 2021; Misra and Froelich, 2012). The output consists of two parts: (1) low-temperature authigenic clay formation, and (2) high-temperature seafloor alteration, which are essentially the same water–rock interaction processes occurring under different temperatures (Seyedali et al., 2021). To avoid adding complexity to the model, we combined them as one output, which is referred to as reverse weathering (see Supplementary Material for more details). Under steady-state conditions, the Li isotope composition of seawater can be calculated by setting the inputs equal to the output (Equation (2)).

$$\delta_{\text{seawater}} = \frac{(F_{\text{river}} \times \delta_{\text{river}} + F_{\text{hydrothermal}} \times \delta_{\text{hydrothermal}} + F_{\text{subduction}} \times \delta_{\text{subduction}})}{F_{\text{sink}}} + \Delta_{\text{seawater-sink}} \quad (2)$$

In this equation, ‘F’ represents flux, and ‘ δ ’ represents isotopic composition (full descriptions of the variables are found in [Table S6](#) and the [Supplementary Materials](#)). We use the Li fluxes and their isotopic compositions, including the weathering flux (F_{river}), hydrothermal flux ($F_{\text{hydrothermal}}$), subduction flux ($F_{\text{subduction}}$), and sink fractionation factor ($\Delta_{\text{seawater-sink}}$), to calculate the Li isotope composition of seawater (δ_{seawater}). In a steady-state scenario, $F_{\text{river}} + F_{\text{hydrothermal}} + F_{\text{subduction}} = F_{\text{sink}}$.

Theoretically, the Devonian rise in the seawater Li isotope record could be explained by changes in any of the inputs or the output (Equation (2)). For example, an abrupt increase in $\Delta_{\text{Li-seawater-sink}}$ by 10 ‰ would be sufficient, by itself, to drive the 10 ‰ increase in $\delta^7\text{Li}$ values. Changes in the sink fractionation factor are believed to be related to the reverse weathering process, which is highly dependent on pH and Si concentrations (Kalderon-Asael et al., 2021). Given that the secular Li isotope increase was monotonic, and that a high $\delta^7\text{Li}$ seawater signature has persisted until today, an increase in the isotopic fractionation of the sink could theoretically have been related to changes in reverse weathering as a result of decreasing ocean Si concentrations. However, it has been suggested that decreases in Si concentrations through time were related to the evolution of radiolarians and/or diatoms, which prospered during the Cambrian and Mesozoic respectively, and therefore were not contemporaneous with the Li isotope increase observed here (Isson and Planavsky, 2018; Mackenzie and Kump, 1995; Trower et al., 2021). Hence, any explanation invoking a sudden change to the sink fractionation factor currently lacks sufficient evidence. On the other hand, the magnitude of the increase in seawater $\delta^7\text{Li}$ values suggested by our data cannot be explained solely by a reduction in the size of the hydrothermal flux or by a similar reduction in the subduction refluxes. In fact, changes to these inputs would likely result in a maximum increase of less than 3 ‰, even if the fluxes were reduced to 0 mol/yr, because these input fluxes (at least in the modern day) have similar isotopic compositions (~6 to 8 ‰ for hydrothermal, and ~5 ‰ for subduction reflux) to the inferred seawater composition (~10 ‰) prior to the Li isotope rise (Fig. 2B). Therefore, unless their past isotopic compositions were substantially different to today, changes to hydrothermal activity or the subduction refluxes would not change the seawater isotopic composition to the degree seen in our data.

After ruling out variations in the other fluxes as major drivers of the observed Li isotope increase, we propose that continental weathering changes are the most appropriate candidate. If the magnitude of the global riverine Li flux remained unchanged across the Devonian period, the mean $\delta^7\text{Li}_{\text{river}}$ value would have needed to increase by considerably more than 10 ‰ (assuming the Early Devonian seawater value was ~5 ‰ (Kalderon-Asael et al., 2021)). Alternatively, if the riverine $\delta^7\text{Li}$ value was equal to the modern-day average (23 ‰), and did not vary through the Devonian period, the global riverine Li flux would have needed to increase by ~14 times. However, the simple IMB method applied above lacks any representation of the dynamic relationship inherent between Li fluxes and Li isotope compositions (Caves Rügenstein et al., 2019; Kalderon-Asael et al., 2021; Li and West, 2014), and thus it is difficult to decipher whether a change in the flux or the isotopic compositions of the continental weathering input was the major contributing factor to the increase in seawater $\delta^7\text{Li}$ values at this time, or whether it was a combination of both (Vigier and Godderis, 2015). Therefore, we introduce an improved Monte Carlo model that not only considers the relationship between Li fluxes and their Li isotopic composition, but is also able to include a wide range of uncertainties for various parameters (see [Tables S6, S7](#)) (Kalderon-Asael et al., 2021). The main construction is

described below, and more details are found in the [Supplementary Materials](#).

The modern ocean residence time of Li is ~1 Myr (Pogge von Strandmann et al., 2013), and a similar residence time for Li might be expected for the Devonian Period. Previous studies therefore used 1 Myr timesteps to build such a model (e.g., Li and West, 2014; Vigier and Godderis, 2015). However, to apply the steady-state equation, we need to ensure that the oceanic Li budget reaches steady state at each time step. Thus, our steady-state box model in this study was built with a longer 3 Myr timestep, with 20 steps between 420 Ma and 360 Ma. This decision is a conservative compromise, reflecting the poor understanding of seawater Li chemistry and reverse weathering processes (which influence the sink of Li) in the Palaeozoic. We run the model as a set of Monte Carlo simulations, with a resampling number set at 2000 times, in order to obtain a sufficient number of trials from which we can infer statistical meaning (Kalderon-Asael et al., 2021).

The previous box modelling study (Kalderon-Asael et al., 2021) randomly sampled the weathering fluxes (F_{river}) and their isotopic compositions (δ_{river}) within a certain range (e.g., F_{river} was sampled from a uniform distribution in the range from 0 to 10 Gmol/yr). In comparison, the key improvement in our model is that we use existing evidence of the relationships between F_{river} and its isotopic composition with temperature, denudation rate, reaction rate, and regolith thickness to calculate their values, with known uncertainties used to constrain their possible ranges (see [Supplementary Materials](#)). In this way, the riverine flux and isotopic values input to the model have a physical basis.

$$W = D \times \left(1 - \exp \left[-K' \left(1 - \exp(r \times q) \right) \times \exp \left(\frac{Ea}{RT_0} - \frac{Ea}{RT} \right) \times \left(\frac{z}{\bar{z}} \right)^{\sigma+1} \right] \right) \quad (3)$$

$$K' = K \times e^{\left(-\frac{z}{z_0} \right)} \quad (4)$$

$$WI = \frac{W}{D} \quad (5)$$

The Li weathering flux (F_{river}) is calculated based on the weathering flux (W), which is itself derived from Equation (3) (see details in the [Supplementary Materials](#) and the parameters in [Tables S6, S7](#)) (West, 2012). In this equation, W is determined by the denudation rate (D , $D = \text{chemical weathering (W)} + \text{physical erosion (E)}$), indicating total amount of material removed in a certain period of time), the reaction rate for fresh rock dissolution (K), surface run-off (q , which is proportional to precipitation (P)), temperature (T), and effective regolith thickness (z). We slightly modified the parameter K , by following Maffre et al. (2022) to add an additional term to consider the decaying reaction rates of rocks with time (denoted as K' ; Equations (3) and (4), where $z_0 = 1.83 \text{ t/m}^2 \approx 2.25 \text{ m}$). Herein, we follow the definition of West (2012) on the ‘regolith’ as the uppermost part of the crust that produces the weathering flux, and thus we do not distinguish between the terms ‘regolith’ and ‘soil’. Hence, this ‘regolith’ term does not equate to the true thickness of regolith. The terms Ea and R are the activation energy and gas constant, respectively, while r and σ are mathematical fitting parameters ([Table S7](#)).

The isotopic compositions of the weathering flux (δ_{river}) are estimated from the observed ‘boomerang’ relationship between weathering intensity (WI ; Equation (5)) and $\delta^7\text{Li}$ values in modern rivers (Dellinger

et al., 2015). This approach considers three mechanisms, including Li release from primary minerals, and both release and removal from secondary minerals. The details of how we capture the non-linear relationship between WI and $\delta^7\text{Li}$ values are given in the [Supplementary Materials](#).

We fed the model by inputting Devonian records of temperature, denudation rates, and other parameters into Equation (3), with their uncertainties, along with a range of possible regolith thicknesses (West., 2012), in order to calculate the W and corresponding Li flux (F_{river}) and its isotopic composition (δ_{river}).

With our modelled Li riverine flux and its isotopic composition, and assuming the other fluxes were within the ranges we set in our Monte Carlo simulation, we generated a set of possible seawater $\delta^7\text{Li}$ curves for the Devonian. Following Kalderon-Asael et al. (2021), we adopted an uncertainty of $\pm 4\text{‰}$ for the reconstructed seawater Li isotope curve (Fig. 5B, black lines), which considers the uncertainties arising from the Li isotope fractionation between carbonate and seawater, as well as

some minor fluid diagenesis. Any modelled runs which did not fit the Li isotope records for the Devonian seawater within those constraints were excluded. The remaining model results, where the set of inputs generated model results that fit the paleo-record (Fig. 5A), are then used to interpret the possible drivers of the Devonian Li isotope rise (i.e., red dots in Fig. 5).

Considering the current understanding of how processes such as denudation and temperature operate upon weathering, combined with the wide uncertainty ranges sampled by our Monte Carlo approach, the box model results suggest that the rise in seawater $\delta^7\text{Li}$ values is best explained by a $\sim 10\text{‰}$ rise in riverine $\delta^7\text{Li}$ values (from $\sim 14\text{‰}$ to $\sim 24\text{‰}$) (Fig. 5D), accompanied by a two-fold increase in riverine Li fluxes across the Mid-Devonian (Fig. 5C). At the same time, the $\Delta^7\text{Li}_{\text{seawater-sink}}$ shows only a minor increase from 4‰ to 5‰ during this time (Fig. 5E), potentially suggesting it was not a major driver of those changes. The increase in riverine Li fluxes and higher $\delta^7\text{Li}$ values were linked to a significant increase in WI from 0.01 to over 0.06 (i.e., similar to present-

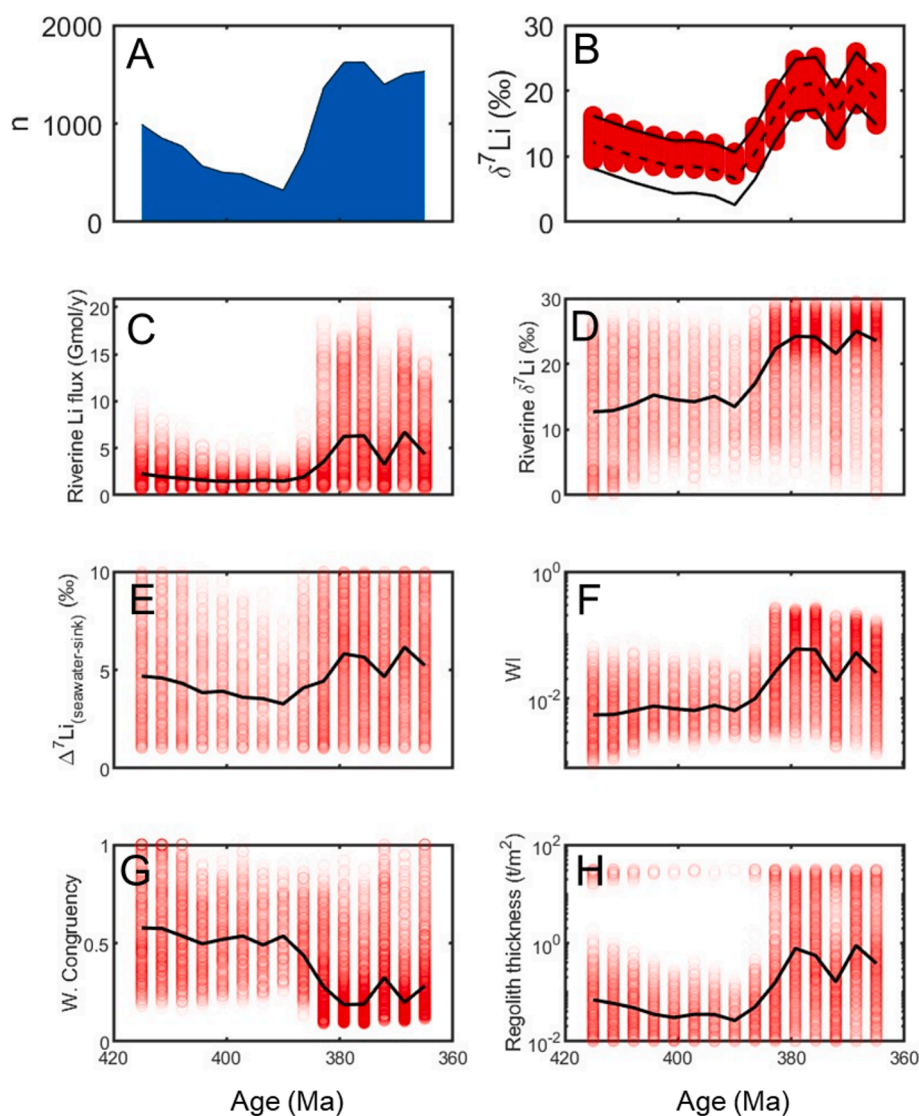


Fig. 5. Outputs from the Li box model. A: The number of runs (out of 2000) for which the model produced results in agreement with the Li isotope record. B: Model results (red dots) which fit the seawater Li isotope paleo-record (black lines). The black solid lines in panel B indicate the upper and lower bounds from the Li isotope records, while the dashed line indicates the average of the Li isotope records. C: Riverine Li flux. D: Riverine Li isotope composition. E: Li isotope fractionation during removal into the Li sink from seawater. F: Weathering Intensity (WI, Equation (5)). G: Weathering congruency (f), defined as the proportion of Li remaining in the fluid after water–rock interaction. H: Regolith thickness (z). The red data points in panels B–H are the results from individual runs that fit within the bounds of the Li isotope records, and the black lines in panels C–H show the median values of the Monte Carlo results. For the purpose of visualisation, we modified the transparency of the red dots: darker red indicates a greater clustering of dots.

day global values) (Fig. 5F) (Caves Rugenstein et al., 2019), and a decline in weathering congruency (i.e., the ratio of primary rock dissolution (congruent) to secondary mineral formation (incongruent)) (Fig. 5G). The change in WI was primarily driven by an increase in weathering (W) compared to denudation (D), i.e., the increase in weathering was of greater magnitude than the increase in denudation rates. Overall, these results indicate that the changes in seawater Li isotope composition could be reasonably explained by changes in continental weathering, moving from a more congruent (kinetic-limited) weathering regime to a more incongruent (supply-limited) weathering regime. In this scenario, the change in WI was likely linked to a change in regolith thickness, which increased in the model from less than 0.1 t/m² to 1 t/m² (Fig. 5H, median value), potentially suggesting that the rise of Li isotopes was driven by the thickening of the regolith. It is also possible that there was very thick (~20 t/m²) regolith in the early Devonian and that the regolith thickness decreased through the mid-Devonian (Fig. 5H, red dots at top), but this scenario is significantly less likely (less clustering of dots).

However, it is important to note that changes in WI, weathering flux, and riverine Li isotopic composition can be influenced by many factors other than regolith thickness (Equation (3)). Although the Monte Carlo method takes into consideration a wide uncertainty range in the input parameters, the distribution of these uncertainties was set to be uniform and to operate independently of each other, which may not necessarily reflect real-world processes. For example, the level of CO₂ in the atmosphere can influence global average temperature, and therefore affect the rock reaction rates and runoff. Therefore, we tested potential co-dependencies in further sensitivity tests, including a varying runoff rate (ratio of q to P), a CO₂ level-controlled reaction rate, and changes in the fractionation factor (see Supplementary Materials). Studies have also emphasised the importance of reverse weathering processes on the Earth system (Li and West, 2014; Isson et al., 2018). Therefore, despite our simple IMB modelling suggesting that changes in the Li sink did not substantially affect the Devonian seawater Li isotope record (see above), we also conducted sensitivity tests for the influence of both climate-dependent and tectono-climate (sediment)-dependent reverse weathering changes on the δ⁷Li record generated by our model. More details of the configurations of these scenarios can be found in the Supplementary Materials. The relatively poorer fitting of all these scenarios (Fig. S6) suggests that, based on our current understanding of the Devonian Period, regolith thickening was very likely the main driver of the weathering transformations, and consequently the δ⁷Li record, across the Devonian (see Supplementary Materials).

Many possible processes could have affected the regolith thickness, including changes in vegetation, climate, slope (tectonics), and lithology (Norton et al., 2014). Therefore, to investigate the overall drivers behind regolith change, we consider four scenarios in this study: (1) it varies independently of abiotic processes (i.e., regolith thickness is not controlled by factors related to climate and/or tectonics, and is solely influenced by biological factors such as plant evolution); (2) slope/tectonic changes alone affect it; (3) climate alone affects it; and (4) slope/tectonics and climate combined affect it. We use the baseline Monte Carlo model (from above) to represent scenario 1 (biology). In scenario 2 (tectonics), we couple the regolith thickness to denudation rates via Equation (6) (Gabet and Mudd, 2009). In scenario 3 (climate), we couple the regolith thickness to the climate (precipitation (P) and temperature (T)) via Equation (7) (Norton et al., 2014). In scenario 4 (tectonics and climate), we use Equation (8) (West, 2012) to couple regolith thickness to both climate and tectonics.

$$z = \frac{\ln\left(\frac{D}{10000}\right)}{-2300} \quad (6)$$

$$z = 0.42P \times \exp\left(\frac{Ea}{RT_0} - \frac{Ea}{RT}\right) \quad (7)$$

$$z = \frac{\ln\left(\frac{D}{10000 \left(1 - \exp(r \times q)\right) \times \exp\left(\frac{Ea}{RT_0} - \frac{Ea}{RT}\right)}\right)}{-2300} \quad (8)$$

The detailed configurations and assumptions of these three additional scenarios can be found in the Supplementary Materials. The resultant poor fitting in all three additional tests (scenarios 2 – 4) appears to suggest that the regolith thickening occurred largely independent of either climate or tectonics (Fig. S7), even though these factors are generally considered as major controls on regolith production. These test results, based on our understanding of the Earth system during the Devonian, may suggest that the increase in Devonian seawater Li isotopes is likely related to independent regolith thickening. As the root-depth evolution of vascular plants is independent from tectonic and climatic evolution, herein, we suggest that the rapid expansion of deep-rooted land plants might have been responsible for the regolith thickening and ultimately the changes in weathering during the Devonian, as also hypothesized by Kalderon-Asael et al. (2021). Indeed, the timing of the increase in our brachiopod δ⁷Li data, and the inferred rise in seawater δ⁷Li values, agrees well with the fossil records of deep-rooted forests found worldwide in the Mid-Devonian (~385 Ma) (Stein et al., 2020) (Fig. 2E). Unlike the avascular dwarf plants of the Ordovician and Silurian, the roots of the Late Devonian arborescent plants could reach several metres in depth, which may have increased the weathering fluxes (Algeo et al., 2001). In addition, these deep roots would have enabled the trees to bind soils, thereby decreasing soil erosion and increasing soil residence times, eventually allowing more time for secondary mineral formation (i.e., higher Li isotope compositions; arrow 1 in Fig. 6).

The above discussion demonstrates that the Devonian Period experienced significant changes in terrestrial silicate weathering, as shown by the reconstructed Li isotope records, and that such changes were likely driven by plant evolution, and specifically by the presence of deep-rooted forests. However, we acknowledge that several assumptions are made to simplify the scenarios in our models, whereas in reality it was likely that multiple changes to the Earth system occurred concurrently. For example, plants can influence continental weathering in ways other than by changing regolith thickness, and in turn the controlling factors on regolith thickness can be influenced by factors other than tectonics, climate, and vegetation, such as through changes in porosity (e.g., Dahl and Arens, 2020; Ehrenfeld et al., 2005). Hence, our model cannot capture all the aspects by which plant evolution in the Devonian could have influenced weathering, and only reflects a broad global scenario with coarse spatial and temporal resolution. Nevertheless, based on the current understanding of the Devonian environment, our new Li isotope reconstruction, and our modelling, we consider regolith thickening by plant root penetration to be the most appropriate explanation. Overall, these results suggest that this indirect role of the biosphere on silicate weathering rates could have been significant in altering global elemental cycles.

4.3. Maintenance of high δ⁷Li_{seawater} values in the Late Devonian and implications for terrestrial-ocean relationships

Given that deep roots bind soils, thereby decreasing erosion rates, their evolution likely lengthened soil and rock residence times on land compared to the small-rooted plants that had evolved before them (Dahl and Arens, 2020). Considering the reactivity (i.e., intrinsic weathering

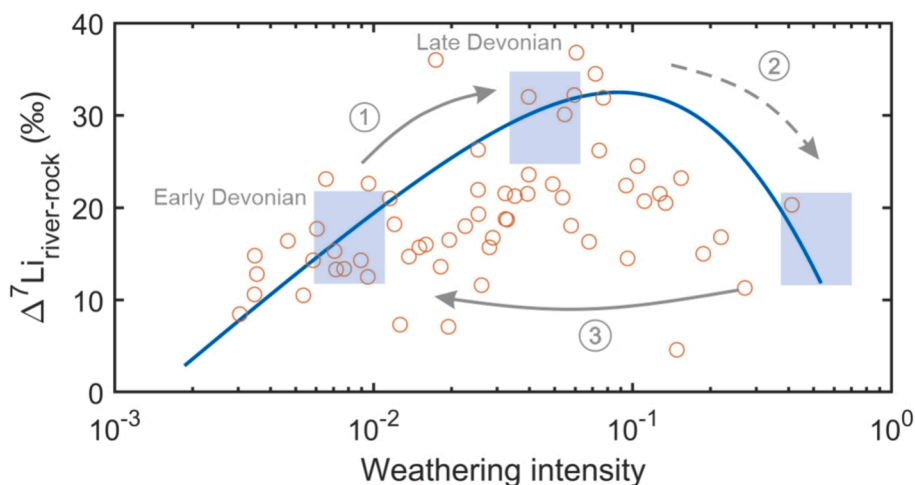


Fig. 6. Relationship between weathering intensity (WI) and $\Delta^7\text{Li}_{\text{river-source rock}}$ values. Circles are modern observations (Dellinger et al., 2015), and the blue curve is the modelled ‘boomerang curve’ in this study. The WI is proposed to increase from less than 0.01 in the Early Devonian to $\sim 0.05\text{--}0.06$ in the Late Devonian through arrow 1 (mainly via regolith thickening). A further increase in regolith thickness would increase the WI and force the system into a supply-limited weathering regime, producing low $\delta^7\text{Li}_{\text{river}}$ values (arrow 2). However, the periodic destruction of forest ecosystems could remove roots and reduce the regolith thickness, re-exposing fresh rocks and helping drive the system back to a kinetic-limited regime (arrow 3). The repeated destruction-regeneration events (arrow 3 to 1 to 2) could help to explain why high $\delta^7\text{Li}_{\text{seawater}}$ values were maintained during the Late Devonian.

rate) of rocks (e.g., Yoo and Mudd, 2008), and that the proportion of reactive minerals in regolith columns decreases with time, a prolonged soil and rock residence time would cause a decline in weathering fluxes (Equation (4)) (Maffre et al., 2022). Therefore, we might expect the weathering rates of primary minerals to have significantly decreased following the Devonian plant colonisation, leading to a high WI regime in which secondary minerals (e.g. clays) start to redissolve, producing riverine fluxes with low $\delta^7\text{Li}$ values and low Li fluxes (Dellinger et al., 2015) (arrow 2 in Fig. 6). This situation would lead to the oceanic Li budget becoming dominated by the hydrothermal input, driving $\delta^7\text{Li}_{\text{seawater}}$ to lower, more mantle-like, values. However, this scenario contradicts both our data and our model observations: the modelled WI did not soar to the high values expected from a strongly supply-limited regime, and the $\delta^7\text{Li}_{\text{seawater}}$ values remained high (20 ‰) during the Late Devonian (Fig. 2B cf. arrow 2 in Fig. 6).

To explain the apparent discrepancy between the Li isotope signatures we would expect, based on modern observations, and the seawater Li isotope compositions reconstructed from Devonian paleo-records, we propose that the repeated destruction and regeneration of terrestrial ecosystems helped to maintain high $\delta^7\text{Li}_{\text{seawater}}$ values during the Late Devonian, thereby circumventing the problem of a reduction in primary mineral availability as soils thicken. Theoretically, if the mature ecosystems are destroyed, the roots binding the soils would be removed, thereby increasing the erosion rates of the overlying regolith and exposing fresh rocks. The continents would then enter a kinetic-limited weathering regime with low WI, producing low $\delta^7\text{Li}_{\text{river}}$ values and high Li fluxes (arrow 3 in Fig. 6). The subsequent regeneration of the ecosystems (i.e., restoration of plants) could gradually rebuild the regolith (arrow 1 in Fig. 6), producing weathering fluxes with highly fractionated $\delta^7\text{Li}_{\text{river}}$ values again. As the regolith thickens, the WI would increase (arrow 2 in Fig. 6), until another destruction event removes the roots and re-exposes the fresh rocks. These destruction-regeneration cycles could have repeated with a high frequency, producing a quasi-stable weathering pattern. Given the long residence time of Li in the ocean, the oscillations in $\delta^7\text{Li}_{\text{river}}$ values and Li fluxes would result in overall high $\delta^7\text{Li}_{\text{seawater}}$ values on million-year timescales (i.e., the oscillations in the inputs over shorter timescales would likely be undetectable in marine sediments). The potential causes of the terrestrial ecosystem destruction required for such a scenario have been studied extensively, and include widespread wildfires, which might have been triggered by orbital variations or volcanic eruptions (De Vleeschouwer et al., 2017;

Lu et al., 2021; Scotese et al., 2021).

As argued above, given the relatively long ocean residence time of Li, these destruction-regeneration cycles may not be discernible in those chemical weathering proxy records (Fig. 2B, C). However, they may have been indirectly recorded by other proxies. For example, charcoal records suggest wildfires became more frequent during the Late Devonian, due to the expansion of lignophytes (Lu et al., 2021). The deposition of black shales in North America may also have recorded these destruction events, as evidenced by the terrestrial woody debris in these shales (Lu et al., 2019). In addition, oscillations in ocean chemistry and oxygen levels during the Mid-Late Devonian, as indicated by carbon and uranium isotopes (Fig. 2G, H), as well as repeated biological events (Fig. 2F), potentially suggest the presence of repeated destruction events (Becker et al., 2020; Elrick et al., 2022). However, further studies integrating weathering proxies, redox proxies, lithology, and organic geochemistry with high temporal resolution, both across the Late Devonian and targeting individual events, are needed to better establish these relationships.

Overall, we can now better place continental weathering into the operation of the Devonian Earth system with the evidence that biologically-driven regolith variations were an important driver of global silicate weathering. During the Early Devonian, shallow-rooted plants could not efficiently recycle the nutrients in their primitive forest ecosystems, due to their relatively weak capability to prevent soil erosion and nutrient loss. Therefore, this simple ecosystem could only be sustained by continuous plant-stimulated primary mineral weathering (Fig. 7A). During the Late Devonian, the oscillating weathering patterns may have caused a temporally heterogeneous supply of nutrients to the ocean due to the repeated destruction-regeneration cycles, contributing to an unstable marine environment (Fig. 7B, C). Such environmental stressors (i.e., changing environment) might also have allowed certain adaptive species (i.e., ecological generalists) to disperse and thrive, thereby reducing the overall biodiversity, resulting in the Late Devonian mass extinctions (Stigall, 2012). In addition, the accompanying influx of secondary minerals derived from soils and the elevated production of organic matter could have promoted the burial of organic carbon in the ocean, potentially making this biotic pathway a relatively more important component of the global carbon cycle.

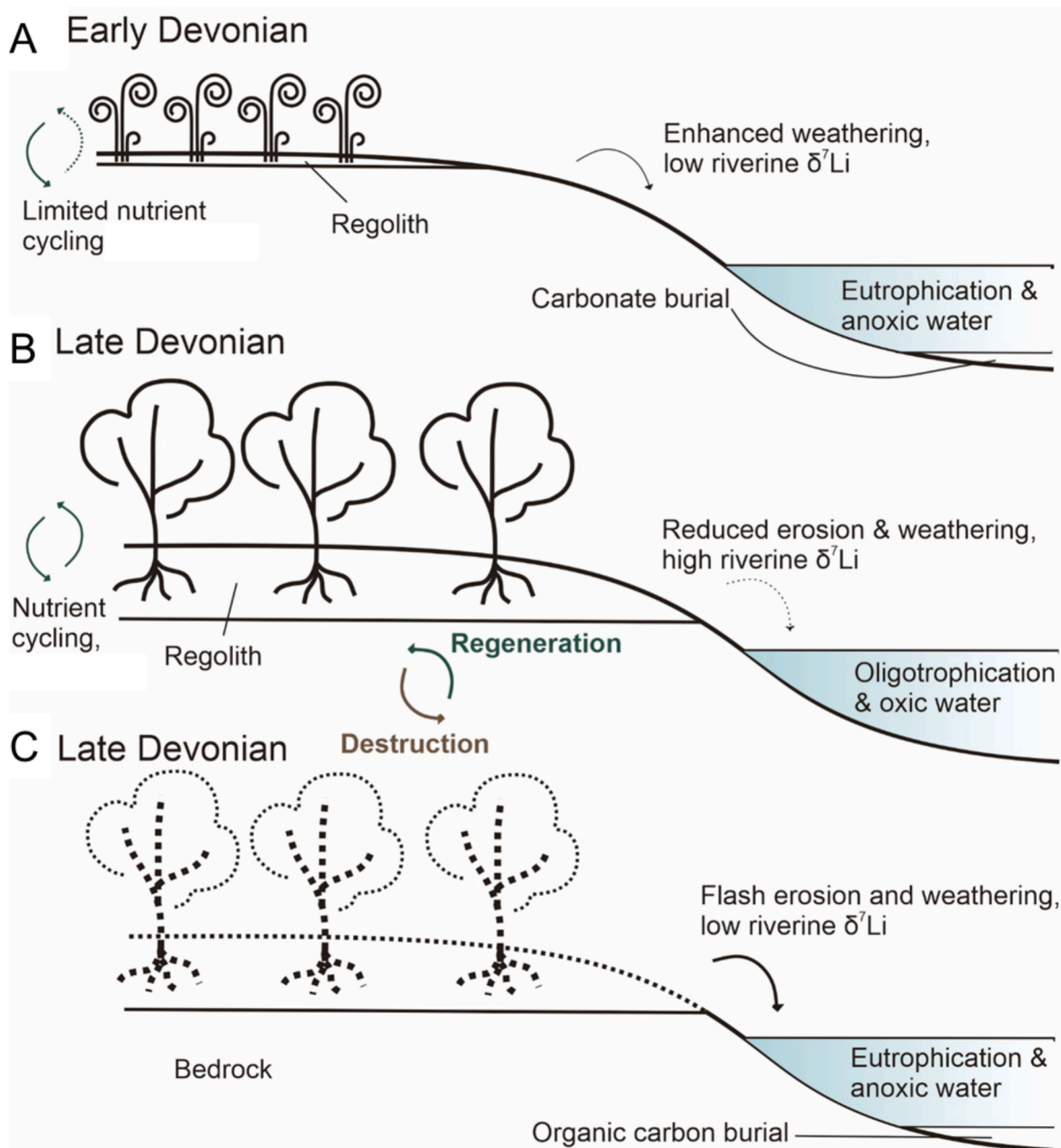


Fig. 7. Cartoon illustrating the pulsed weathering pattern induced by terrestrial ecosystem destruction-regeneration cycles. A: In the Early Devonian, shallow-rooted and non-vascular plants had a limited effect on soil retention and did not efficiently recycle nutrients. The lost nutrients were transferred into the ocean, promoting carbonate burial, primary production, eutrophication, and ocean anoxia. B: In the Late Devonian, during the regeneration stage, deep-rooted vascular plants reduced soil erosion, leading to a thicker regolith, and more efficiently recycled nutrients. Plants are not driven to weather rocks under these conditions, because they are no longer in an aggrading status and could obtain nutrients via recycling. The reduced flux of nutrients to the ocean resulted in oligotrophy and ultimately oxic seawater. C: In the Late Devonian, after the destruction stage, the disappearance of plants allowed the enhanced erosion of soils. The nutrients and organic carbon stored in the soils were rapidly transported to the ocean, creating flash eutrophication and anoxia of seawater, and promoting organic carbon burial. The regeneration and destruction were possibly cyclical, recurring multiple times during the Late Devonian, resulting in pulsed weathering patterns, but likely occurred too quickly to be detectable via the ocean Li isotope record, due to buffering by its long ocean residence time.

5. Conclusions

Based on the marine carbonate samples identified to represent robust seawater archives, a relatively rapid increase in seawater Li isotope composition of around 10 ‰ in 10 million years is observed during the Mid-Devonian. A new Li isotope box model was constructed to investigate the drivers of this Li isotope shift, and it suggests that an increase in both global weathering intensity and regolith thickness occurred at this time. We attribute these changes to the widespread colonisation of the continents by deep-rooted plants, which would have enhanced chemical

weathering and led to the production of thicker soils. The expansion of deep-rooted plants likely led to an increase in the recycling of nutrients on the continents, creating more complex terrestrial ecosystems. The repeated destruction and regeneration of this terrestrial ecosystem may have not only sustained high riverine $\delta^7\text{Li}$ values and relatively high dissolved Li fluxes (and hence high seawater $\delta^7\text{Li}$ values), but could also have contributed to the gradual loss of marine species during the Late Devonian and shifted the main carbon burial sink towards biotic pathways.

CRediT authorship contribution statement

Xianyi Liu: Writing – review & editing, Writing – original draft, Visualization, Software, Project administration, Methodology, Investigation, Formal analysis, Data curation, Conceptualization. **Alexander J. Krause:** Writing – review & editing, Validation, Supervision, Software. **David J. Wilson:** Writing – review & editing, Supervision, Investigation. **Wesley T. Fraser:** Writing – review & editing, Supervision, Investigation. **Michael M. Joachimski:** Writing – review & editing, Resources. **Uwe Brand:** Writing – review & editing, Resources. **Alycia L. Stigall:** Writing – review & editing, Resources. **Wenkun Qie:** Writing – review & editing, Resources. **Bo Chen:** Writing – review & editing, Resources. **Xiangrong Yang:** Writing – review & editing, Resources. **Philip A.E. Pogge von Strandmann:** Writing – review & editing, Supervision, Investigation, Funding acquisition, Conceptualization.

Data availability

All the geochemical data generated in this study can be found in the Excel file in the Figshare database (<https://doi.org/10.6084/m9.figshare.25659156>) or the Zenodo database (<https://zenodo.org/records/14624557>). The model code (in MATLAB 2020) is available at: <http://github.com/xyl96/Devonian-weathering-model>.

Declaration of competing interest

The authors declare that they have no known competing financial interests or personal relationships that could have appeared to influence the work reported in this paper.

Acknowledgements

P.P.v.S. and A.J.K. are supported by ERC grant 682760 CON-TROPASTCO₂, which also supported analyses. D.J.W. is supported by a Natural Environment Research Council independent research fellowship (NE/T011440/1). U.B. thanks the Natural Science and Engineering Research Council of Canada (NSERC) for continued support. Q.W. and B. C. are supported by the Second Tibetan Plateau Scientific Expedition and Research Program (2019QZKK0706), and Strategic Priority Research Program (B) of Chinese Academy of Sciences (Grant No. XDB26000000). Gary Tarbuck is thanked for assistance with the concentration and isotope measurements, and Dr. Chunyao Liu is thanked for help with the Li isotope purification process. Dr. Xu (Yvon) Zhang and Dr. Chaoyi Lu are also thanked for their constructive advice. Thanks BEIF at UCL for help analysing Oxygen and Carbon isotopes. Special thanks to Prof. Matthew Fantle and two anonymous reviewers for their advice that significantly improved the presentation of the manuscript. For the purpose of open access, the author has applied a 'Creative Commons Attribution (CC BY) licence' to any Author Accepted Manuscript version arising.

Appendix A. Supplementary material

The Excel tables in the supplementary material contains the data we used in the manuscript, including measured data (elemental concentrations and Li isotopes) and model parameters. These data are also deposited in Zenodo and Figshare (see Data availability). The PDF document in the supplementary material includes details about the diagenesis model, a description of the model configuration, and the results of sensitivity tests. Supplementary material to this article can be found online at <https://doi.org/10.1016/j.gca.2025.02.036>.

References

- Algeo, T.J., Scheckler, S.E., 1998. Terrestrial-marine teleconnections in the Devonian: links between the evolution of land plants, weathering processes, and marine anoxic events. *Philos. Trans. R. Soc. Lond. B Biol. Sci.* 353 (1365), 113–130.
- Algeo, T.J., Scheckler, S.E., Maynard, J.B., 2001. 12. Effects of the Middle to Late Devonian Spread of Vascular Land Plants on Weathering Regimes, Marine Biotas, and Global Climate, Plants invade the land. Columbia University Press, pp. 213–236.
- Andrews, E., von Strandmann, P.A.P., Fantle, M.S., 2020. Exploring the importance of authigenic clay formation in the global Li cycle. *Geochim. Cosmochim. Acta* 289, 47–68.
- Barash, M., 2016. Causes of the great mass extinction of marine organisms in the Late Devonian. *Oceanology* 56, 863–875.
- Bastian, L., Vigier, N., Reynaud, S., Kerros, M.-E., Revel, M., Bayon, G., 2018. Lithium Isotope Composition of Marine Biogenic Carbonates and Related Reference Materials. *Geostand. Geoanal. Res.* 42 (3), 403–415.
- Becker, R.T., Königshof, P., Brett, C.E., 2016. Devonian climate, sea level and evolutionary events: an introduction. *Geol. Soc. Lond. Spec. Publ.* 423 (1), 1.
- Becker, R.T., Marshall, J.E.A., Da Silva, A.C., Agterberg, F.P., Gradstein, F.M., Ogg, J.G., 2020. Chapter 22 - The Devonian Period. In: Gradstein, F.M., Ogg, J.G., Schmitz, M. D., Ogg, G.M. (Eds.), *Geologic Time Scale 2020*. Elsevier, pp. 733–810.
- Brand, U., 1989. Global climatic changes during the Devonian-Mississippian: Stable isotope biogeochemistry of brachiopods. *Global Planet. Change* 1 (4), 311–329.
- Cascales-Miñana, B., 2016. Apparent changes in the Ordovician-Mississippian plant diversity. *Rev. Palaeobot. Palynol.* 227, 19–27.
- Caves Rugenstein, J.K., Ibarra, D.E., von Blanckenburg, F., 2019. Neogene cooling driven by land surface reactivity rather than increased weathering fluxes. *Nature* 571 (7763), 99–102.
- Chanda, P., Kohli, A., Teng, F.Z., Fantle, M.S., 2023. Clay authigenesis in carbonate-rich sediments and its impact on carbonate diagenesis. *Geochim. Cosmochim. Acta* 346, 76–101.
- Chen, B., Ma, X., Mills, B.J.W., Qie, W., Joachimski, M.M., Shen, S., Wang, C., Xu, H., Wang, X., 2021. Devonian paleoclimate and its drivers: A reassessment based on a new conodont $\delta^{18}O$ record from South China. *Earth Sci. Rev.* 222, 103814.
- Copper, P., Scotese, C.R., 2003. Megareefs in Middle Devonian supergreenhouse climates.
- Cramer, B.D., Jarvis, I., 2020. Chapter 11 - Carbon Isotope Stratigraphy. In: Gradstein, F. M., Ogg, J.G., Schmitz, M.D., Ogg, G.M. (Eds.), *Geologic Time Scale 2020*. Elsevier, pp. 309–343.
- Dahl, T.W., Arens, S.K.M., 2020. The impacts of land plant evolution on Earth's climate and oxygenation state – An interdisciplinary review. *Chem. Geol.* 547, 119665.
- De Vleeschouwer, D., Da Silva, A.-C., Sinnesael, M., Chen, D., Day, J.E., Whalen, M.T., Guo, Z., Claeys, P., 2017. Timing and pacing of the Late Devonian mass extinction event regulated by eccentricity and obliquity. *Nat. Commun.* 8 (1), 1–11.
- Dellinger, M., Gaillardet, J., Bouchez, J., Calmels, D., Louvat, P., Dosseto, A., Gorge, C., Alanoca, L., Maurice, L., 2015. Riverine Li isotope fractionation in the Amazon River basin controlled by the weathering regimes. *Geochim. Cosmochim. Acta* 164, 71–93.
- Dellinger, M., Hardisty, D.S., Planavsky, N.J., Gill, B.C., Kalderson-Asael, B., Asael, D., Croissant, T., Swart, P.K., West, A.J., 2020. The effects of diagenesis on lithium isotope ratios of shallow marine carbonates. *Am. J. Sci.* 320 (2), 150–184.
- Dellinger, M., West, A.J., Paris, G., Adkins, J.F., von Strandmann, P.A.P., Ullmann, C.V., Eagle, R.A., Freitas, P., Bagard, M.-L., Ries, J.B., 2018. The Li isotope composition of marine biogenic carbonates: Patterns and Mechanisms. *Geochim. Cosmochim. Acta* 236, 315–335.
- Demicco, R.V., Lowenstein, T.K., Hardie, L.A., Spencer, R.J., 2005. Model of seawater composition for the Phanerozoic. *Geology* 33 (11), 877–880.
- Ehrenfeld, J.G., Ravit, B., Elgersma, K., 2005. Feedback in the plant-soil system. *Annu. Rev. Environ. Resour.* 30, 75–115.
- Elrick, M., Gilleaudeau, G.J., Romaniello, S.J., Algeo, T.J., Morford, J.L., Sabbatino, M., Goepfert, T.J., Cleal, C., Cascales-Miñana, B., Chernyavskiy, P., 2022. Major Early-Middle Devonian oceanic oxygenation linked to early land plant evolution detected using high-resolution U isotopes of marine limestones. *Earth Planet. Sci. Lett.* 581, 117410.
- Fan, J., Shen, S., Erwin, D.H., Sadler, P.M., MacLeod, N., Cheng, Q., Hou, X., Yang, J., Wang, X., Wang, Y., 2020. A high-resolution summary of Cambrian to Early Triassic marine invertebrate biodiversity. *Science* 367 (6475), 272–277.
- Fantle, M., Lloyd, M., 2025. Demystifying diagenesis: The future of diagenetic inquiry in the geosciences. In A. Anbar and D. Weis (Eds.), *Treatise on Geochemistry* (3rd ed.), v. 2, pp. 249–314.
- Fantle, M.S., Barnes, B.D., Lau, K.V., 2020. The role of diagenesis in shaping the geochemistry of the marine carbonate record. *Annu. Rev. Earth Planet. Sci.* 48, 549–583.
- Foster, G.L., Royer, D.L., Lunt, D.J., 2017. Future climate forcing potentially without precedent in the last 420 million years. *Nat. Commun.* 8 (1), 14845.
- Füger, A., Konrad, F., Leis, A., Dietzel, M., Mavromatis, V., 2019. Effect of growth rate and pH on lithium incorporation in calcite. *Geochim. Cosmochim. Acta* 248, 14–24.
- Gabet, E.J., Mudd, S.M., 2009. A theoretical model coupling chemical weathering rates with denudation rates. *Geology* 37 (2), 151–154.
- Hathorne, E.C., James, R.H., 2006. Temporal record of lithium in seawater: A tracer for silicate weathering? *Earth Planet. Sci. Lett.* 246 (3), 393–406.
- Hindshaw, R.S., Tosca, R., Goût, T.L., Farnan, I., Tosca, N.J., Tipper, E.T., 2019. Experimental constraints on Li isotope fractionation during clay formation. *Geochim. Cosmochim. Acta* 250, 219–237.
- Isson, T.T., Planavsky, N.J., 2018. Reverse weathering as a long-term stabilizer of marine pH and planetary climate. *Nature* 560 (7719), 471–475.

- Joachimski, M.M., Buggisch, W., 2002. Conodont apatite $\delta^{18}\text{O}$ signatures indicate climatic cooling as a trigger of the Late Devonian mass extinction. *Geology* 30 (8), 711–714.
- Kalderon-Asael, B., Katchinoff, J.A.R., Planavsky, N.J., Hood, A.V.S., Dellinger, M., Bellefroid, E.J., Jones, D.S., Hofmann, A., Ossa, F.O., Macdonald, F.A., Wang, C., Isson, T.T., Murphy, J.G., Higgins, J.A., West, A.J., Wallace, M.W., Asael, D., Pogge von Strandmann, P.A.E., 2021. A lithium-isotope perspective on the evolution of carbon and silicon cycles. *Nature* 595 (7867), 394–398.
- Langmuir, C.H., Vocke, R.D., Hanson, G.N., Hart, S.R., 1978. A general mixing equation with applications to Icelandic basalts. *Earth Planet. Sci. Lett.* 37 (3), 380–392.
- Lenton, T.M., Dahl, T.W., Daines, S.J., Mills, B.J.W., Ozaki, K., Saltzman, M.R., Porada, P., 2016. Earliest land plants created modern levels of atmospheric oxygen. *Proc. Natl. Acad. Sci.* 113 (35), 9704.
- Li, G., West, A.J., 2014. Evolution of Cenozoic seawater lithium isotopes: Coupling of global denudation regime and shifting seawater sinks. *Earth Planet. Sci. Lett.* 401, 284–293.
- Lu, M., Ikejiri, T., Lu, Y., 2021. A synthesis of the Devonian wildfire record: Implications for paleogeography, fossil flora, and paleoclimate. *Palaeogeogr. Palaeoclimatol. Palaeoecol.* 571, 110321.
- Lu, M., Lu, Y., Ikejiri, T., Hoganamp, N., Sun, Y., Wu, Q., Carroll, R., Çemen, I., Pashin, J., 2019. Geochemical evidence of first forestation in the southernmost Euramerica from Upper Devonian (Famennian) black shales. *Sci. Rep.* 9 (1), 1–15.
- Mackenzie, F.T., Kump, L.R., 1995. Reverse Weathering, Clay Mineral Formation, and Oceanic Element Cycles. *Science* 270 (5236), 586.
- Maffre, P., Godderis, Y., Pohl, A., Donnadieu, Y., Carretier, S., Le Hir, G., 2022. The complex response of continental silicate rock weathering to the colonization of the continents by vascular plants in the Devonian. *Am. J. Sci.* 322 (3), 461–492.
- Marriott, C.S., Henderson, G.M., Crompton, R., Staubwasser, M., Shaw, S., 2004. Effect of mineralogy, salinity, and temperature on Li/Ca and Li isotope composition of calcium carbonate. *Chem. Geol.* 212 (1), 5–15.
- McArthur, J., Howarth, R., Shields, G., 2012. Strontium isotope stratigraphy. *The Geologic Time Scale* 1, 127–144.
- McArthur, J.M., Howarth, R.J., Shields, G.A., Zhou, Y., 2020. Chapter 7 - Strontium Isotope Stratigraphy. In: Gradstein, F.M., Ogg, J.G., Schmitz, M.D., Ogg, G.M. (Eds.), *Geologic Time Scale 2020*. Elsevier, pp. 211–238.
- McGhee, G.R., Racki, G., 2012. Extinction: Late Devonian Mass Extinction. eLS (Ed.) doi 10.9780470015902, a0001653.
- Mills, B.J., Scotese, C.R., Walding, N.G., Shields, G.A., Lenton, T.M., 2017. Elevated CO₂ degassing rates prevented the return of Snowball Earth during the Phanerozoic. *Nat. Commun.* 8 (1), 1–7.
- Misra, S., Froelich, P.N., 2012. Lithium Isotope History of Cenozoic Seawater: Changes in Silicate Weathering and Reverse Weathering. *Science* 335 (6070), 818–823.
- Norton, K.P., Molnar, P., Schlunegger, F., 2014. The role of climate-driven chemical weathering on soil production. *Geomorphology* 204, 510–517.
- Penniston-Dorland, S., Liu, X.-M., Rudnick, R.L., 2017. Lithium Isotope Geochemistry. *Rev. Mineral. Geochem.* 82 (1), 165–217.
- Percival, L.M.E., Selby, D., Bond, D.P.G., Rakociński, M., Racki, G., Marynowski, L., Adatte, T., Spangenberg, J.E., Föllmi, K.B., 2019. Pulses of enhanced continental weathering associated with multiple Late Devonian climate perturbations: Evidence from osmium-isotope compositions. *Palaeogeogr. Palaeoclimatol. Palaeoecol.* 524, 240–249.
- Pistiner, J.S., Henderson, G.M., 2003. Lithium-isotope fractionation during continental weathering processes. *Earth Planet. Sci. Lett.* 214 (1), 327–339.
- Pogge von Strandmann, P.A.E., Fraser, W.T., Hammond, S.J., Tarbuck, G., Wood, I.G., Oelkers, E.H., Murphy, M.J., 2019a. Experimental determination of Li isotope behaviour during basalt weathering. *Chem. Geol.* 517, 34–43.
- Pogge von Strandmann, P.A.E., Jenkyns, H.C., Woodfine, R.G., 2013. Lithium isotope evidence for enhanced weathering during Oceanic Anoxic Event 2. *Nat. Geosci.* 6 (8), 668–672.
- Pogge von Strandmann, P.A.E., Liu, X., Liu, C.-Y., Wilson, D.J., Hammond, S.J., Tarbuck, G., Aristilde, L., Krause, A.J., Fraser, W.T., 2022. Lithium isotope behaviour during basalt weathering experiments amended with organic acids. *Geochim. Cosmochim. Acta* 328, 37–57.
- Pogge von Strandmann, P.A.E., Schmidt, D.N., Planavsky, N.J., Wei, G., Todd, C.L., Baumann, K.-H., 2019b. Assessing bulk carbonates as archives for seawater Li isotope ratios. *Chem. Geol.* 530, 119338.
- Rode, A.L., Lieberman, B.S., 2004. Using GIS to unlock the interactions between biogeography, environment, and evolution in Middle and Late Devonian brachiopods and bivalves. *Palaeogeogr. Palaeoclimatol. Palaeoecol.* 211 (3–4), 345–359.
- Scotese, C.R., Song, H., Mills, B.J., van der Meer, D.G., 2021. Phanerozoic paleotemperatures: The earth's changing climate during the last 540 million years. *Earth Sci. Rev.* 103503.
- Seyedali, M., Coogan, L., Gillis, K., 2021. Li-isotope exchange during low-temperature alteration of the upper oceanic crust at DSDP Sites 417 and 418. *Geochim. Cosmochim. Acta* 294, 160–173.
- Smart, M.S., Filippelli, G., Gilhooly III, W.P., Ozaki, K., Reinhard, C.T., Marshall, J.E., Whiteside, J.H., 2023. The expansion of land plants during the Late Devonian contributed to the marine mass extinction. *Commun. Earth Environ.* 4 (1), 449.
- Stein, W.E., Berry, C.M., Morris, J.L., Hernick, L.V., Mannolini, F., Ver Straeten, C., Landing, E., Marshall, J.E.A., Wellman, C.H., Beerling, D.J., Leake, J.R., 2020. Mid-Devonian Archaeopteris Roots Signal Revolutionary Change in Earliest Fossil Forests. *Curr. Biol.* 30 (3), 421–431.e422.
- Stigall, A.L., 2012. Speciation collapse and invasive species dynamics during the Late Devonian “Mass Extinction”. *GSA Today* 22 (1), 4–9.
- Trower, E.J., Strauss, J.V., Sperling, E.A., Fischer, W.W., 2021. Isotopic analyses of Ordovician–Silurian siliceous skeletons indicate silica-depleted Paleozoic oceans. *Geobiology* 19 (5), 460–472.
- Ullmann, C., Frei, R., Korte, C., Lüter, C., 2017. Element/Ca, C and O isotope ratios in modern brachiopods: Species-specific signals of biomineralization. *Chem. Geol.* 460, 15–24.
- Ullmann, C.V., Campbell, H.J., Frei, R., Hesselbo, S.P., von Strandmann, P.A.P., Korte, C., 2013. Partial diagenetic overprint of Late Jurassic belemnites from New Zealand: Implications for the preservation potential of $\delta^{7}\text{Li}$ values in calcite fossils. *Geochim. Cosmochim. Acta* 120, 80–96.
- Ullmann, C.V., Korte, C., 2015. Diagenetic alteration in low-Mg calcite from macrofossils: a review. *Geological Quarterly* 59 (1), 3–20.
- van Geldern, R., Joachimski, M.M., Day, J., Jansen, U., Alvarez, F., Yolkin, E.A., Ma, X.P., 2006. Carbon, oxygen and strontium isotope records of Devonian brachiopod shell calcite. *Palaeogeogr. Palaeoclimatol. Palaeoecol.* 240 (1), 47–67.
- Vigier, N., Decarreau, A., Millot, R., Carignan, J., Petit, S., France-Lanord, C., 2008. Quantifying Li isotope fractionation during smectite formation and implications for the Li cycle. *Geochim. Cosmochim. Acta* 72 (3), 780–792.
- Vigier, N., Godderis, Y., 2015. A new approach for modeling Cenozoic oceanic lithium isotope paleo-variations: the key role of climate. *Clim. Past* 11 (4), 635–645.
- Vigier, N., Rollion-Bard, C., Levenson, Y., Erez, J., 2015. Lithium isotopes in foraminifera shells as a novel proxy for the ocean dissolved inorganic carbon (DIC). *C. R. Geosci.* 347 (1), 43–51.
- Washington, K.E., West, A.J., Kalderon-Asael, B., Katchinoff, J.A.R., Stevenson, E.I., Planavsky, N.J., 2020. Lithium isotope composition of modern and fossilized Devonian brachiopods. *Geology* 48 (11), 1058–1061.
- West, A.J., 2012. Thickness of the chemical weathering zone and implications for erosional and climatic drivers of weathering and for carbon-cycle feedbacks. *Geology* 40 (9), 811–814.
- Williams, S., Wright, N.M., Cannon, J., Flament, N., Müller, R.D., 2021. Reconstructing seafloor age distributions in lost ocean basins. *Geosci. Front.* 12 (2), 769–780.
- Willis, K., McElwain, J., 2014. The evolution of plants. Oxford University Press.
- Yoo, K., Mudd, S.M., 2008. Discrepancy between mineral residence time and soil age: Implications for the interpretation of chemical weathering rates. *Geology* 36 (1), 35–38.
- Yoshimura, T., Tamenori, Y., Suzuki, A., Kawahata, H., Iwasaki, N., Hasegawa, H., Nguyen, L.T., Kuroyanagi, A., Yamazaki, T., Kuroda, J., Ohkouchi, N., 2017. Altrivalent substitution of sodium for calcium in biogenic calcite and aragonite. *Geochim. Cosmochim. Acta* 202, 21–38.
- Zhang, F., Dellinger, M., Hilton, R.G., Yu, J., Allen, M.B., Densmore, A.L., Sun, H., Jin, Z., 2022a. Hydrological control of river and seawater lithium isotopes. *Nat. Commun.* 13 (1), 3359.
- Zhang, X., Gaillardet, J., Barrier, L., Bouchez, J., 2022b. Li and Si isotopes reveal authigenic clay formation in a palaeo-delta. *Earth Planet. Sci. Lett.* 578, 117339.
- Zhang, X., Saldi, G.D., Schott, J., Bouchez, J., Kuessner, M., Montouillout, V., Henehan, M., Gaillardet, J., 2021. Experimental constraints on Li isotope fractionation during the interaction between kaolinite and seawater. *Geochim. Cosmochim. Acta* 292, 333–347.